

<https://doi.org/10.15407/ujpe67.3.161>

V.F. GEDEON, V.YU. LAZUR, S.V. GEDEON, O.V. YEHAZARIAN

Uzhhorod National University

(54, Voloshyna Str., Uzhhorod 88000, Ukraine; e-mail: volodymyr.lazur@uzhnu.edu.ua)

## RESONANCE STRUCTURE OF CROSS-SECTIONS OF SLOW-ELECTRON SCATTERING BY CALCIUM ATOM

---

*The extended BSR-version of the R-matrix method has been applied to systematically analyze the electron scattering by neutral calcium atoms at collision energies up to 4.3 eV. The strong coupling method with the sets of term-dependent nonorthogonal orbitals and the spline representation of the basis functions are used to accurately represent the target wave functions. The strong-coupling expansion included 39 bound states of the neutral calcium atom, which cover all its states from the ground one to  $4s8s\ ^1S$ . The complex resonance structure of the angle-integrated total cross-sections of the elastic  $e+\text{Ca}$  scattering and the electron-impact excitation of the  $4s4p\ ^3P^o$ ,  $3d4s\ ^3D^e$ ,  $3d4s\ ^1D^e$ ,  $4s4p\ ^1P^o$ , and  $4s5s\ ^3S^e$  states of a Ca atom are studied in detail. The observed structures are associated with particular autodetachment states of the "incident electron + Ca atom" system. The positions and widths of detected resonances are determined, and their spectroscopic classification is carried out.*

*Keywords:* electron, calcium atom, scattering, excitation, ionization, R-matrix with B-splines method, nonorthogonal orbitals, resonances.

### 1. Introduction

The study of the elementary processes taking place at electron collisions with calcium atoms is of considerable interest for a number of reasons. First, the information on parameters of the elementary interaction processes between electrons and Ca atoms is highly required for the successful development of a lot of directions in modern physics and new technologies, including plasma physics, astrophysics, upper atmosphere physics, and thermonuclear power engineering. In particular, calcium produced in the course of supernova explosions is the most used element, when quantitatively analyzing the star spectrum [1]. Ca atoms also have attractive properties for their application in optical frequency standards [2]. In addition, after the activity dealing with controlled thermonu-

clear fusion had been started, there arose an urgent necessity in a better understanding of the basic processes (elastic scattering, excitation, and ionization) taking place at collisions of electrons with Ca atoms [3, 4]. However, for most alkaline earth elements, including calcium, the information on the cross-sections of the elastic scattering and excitation of energy levels in their atoms by the electron impact still remains limited.

Second, the calcium atom with its ground-state configuration  $[1s^2 2s^2 2p^6 3s^2 3p^6] \times (4s^2)\ ^1S$ , as well as the single- and double-excited states  $[1s^2 \dots 3p^6] \times (4snl, 3dnl, 4pnl)\ ^3,^1L$ , is similar in many respects to the helium one. That is, under certain conditions, it can be considered in the framework of the model of two electrons above the Ar-like  $[1s^2 \dots 3p^6]$ -core. Valence and covalent correlations are important for both the ground and low-located excited Ca states. The widely used method for taking covalent correlations

---

© V.F. GEDEON, V.YU. LAZUR, S.V. GEDEON,  
O.V. YEHAZARIAN, 2022

ISSN 2071-0194. Ukr. J. Phys. 2022. Vol. 67, No. 3

into account is based on the application of a semi-empirical copolarization potential [5]. Although this potential strongly simplifies calculations and allows the excitation energies and oscillator strengths to be determined with sufficient accuracy, the question remains as to how accurately the model potential can mimic the covalent correlation, including the non-local and non-dipole contributions. For this reason, correlation effects are taken into account in our approach [6–13] (see Section 2) by including special additional electronic configurations with an excited core into the expansion of the target states and pseudostates.

Third, the atoms of alkaline earth elements are characterized by high polarizability values. Therefore, there arises a necessity to accurately take the high polarizability of the Ca atom into account. In our work [6], it was found that the polarization of the Ca atom in the ground state is determined to a great extent by the strong dipole excitation of the level  $4s4p\ ^1P^o$ . An adequate method allowing the polarization effects to be taken into consideration will be discussed in more detail in the next section, in connection with the issue concerning the resonant scattering of slow electrons by Ca atoms.

Finally, it was found in the experimental [14] and theoretical [15] works that the  $4s^24p\ ^2P_{1/2}$  state of the negative calcium ion,  $\text{Ca}^-$ , is stable rather than resonance as was previously thought. Therefore, it is worth returning to the problem of theoretical description of resonance phenomena occurring at collisions of slow electrons with Ca atoms. This task requires that new concepts and new methods allowing the resonance effects to be taken into account should be implied in order to overcome the current, unsatisfactory state of the theory. Modifications and specifications of the  $R$ -matrix theory and the strong channel coupling method, which are required for this purpose, are presented in section 2.

The study of the resonance structure of the  $e + A$  scattering cross sections is a fundamental problem for the physics of electron-atom collisions. This structure testifies to the existence of quasistationary autoionization states (AISs) – in the case of neutral atoms, these are autodetachment states (ADSs) – of the “target + incident electron” system, the Auger decay of which leads to a complicated resonance structure of scattering cross-sections. As a rule, two types of resonances are observed in scattering cross-sections (see,

e.g., works [16, 17]), which are called the Feshbach and shape resonances. The mechanism of appearance of Feshbach resonances consists in the capture of the incident electron in an AIS by the target in one of its closed channels. However, the electron can be temporarily captured by the target in an open channel as well. The relevant condition is the presence of the potential with a specific shape in a certain open channel. Namely, behind a rather wide barrier, there should be a well with sufficient depth and width, in which the scattered electron would become temporarily bound in the AIS.

Besides the importance of ADSs (AISs) in the electron-atom (ion) scattering processes, these states also play an essential role in plasma and solids. In plasma, as a result of collisions between electrons and atoms (ions), intensive excitation of the ADSs (AISs) in the  $e + A$  system takes place, which affects the energy balance in plasma, thus being a convenient tool for its diagnosis. In solids, there may occur cases where conduction electrons interact with impurity atoms (ions) of the crystal lattice via the formation of ADSs (AISs) and, as a result, this interaction has a resonance character. Beam experiments in which the energy and angular dependences of the cross-sections of elastic scattering, excitation, and atomic (ionic) ionization by electron impact are measured serve as an experimental basis for elucidating the nature of the resonance structure of scattering cross-sections. Relevant experiments for  $e + \text{Ca}$  scattering were performed in works [18–20] and their results will be reported below in the course of systematic presentation of the results of BSR calculations.

In this paper, to study the resonance effects occurring at the collisions of slow electrons with Ca atoms, we used a new version of the  $R$ -matrix method [briefly, the  $B$ -Spline  $R$ -matrix (BSR) method], which was developed in works [6–13, 21–26]. In the framework of this version, a new method was proposed to take resonance effects into account. It is based on the application of term-dependent nonorthogonal orbitals and spline representations for basis functions. The proposed method is free from many of the disadvantages inherent to earlier known methods that are used to make allowance for resonance effects (see, for example, works [16, 17] and references therein) associated with the introduction of a special additional quadratic integrable correlation functions  $\chi_j^\Gamma$  into the expansion of the total wave func-

tion for the  $(N + 1)$ -electron system “atom + incident electron”. This procedure is known to often lead to the appearance of a non-physical pseudoresonance structure in  $e + A$  scattering cross-sections and to a substantial increase in the number algebraic or integro-differential equations that are to be solved.

The analysis of resonances in  $e + A$  scattering is often based on the single-level Breit–Wigner formula for isolated (non-overlapping) resonances. However, in the case of two resonance states with close energies in the same partial wave, the determination of resonance parameters becomes quite a difficult task and requires the generalization of the single-level Breit–Wigner formalism to the multichannel case. Among plenty of other methods that are widely used in the literature to calculate and analyze the parameters of complicated resonance structures in multichannel systems, the most reliable turned out the method developed in the works by Shimamura *et al.* [27–30]. It is based on the concept of “complete separation of resonance and nonresonance channel spaces” and uses the properties of the eigenphase sum and its energy derivative. Both the latest developments of this method [31] and its application in various domains of collision physics (see, e.g., work [32]) testify to the importance and relevance of this approach. Just the latter together with the BSR version of the  $R$ -matrix method was used in this work to study the complicated resonance structure of  $e + \text{Ca}$  scattering cross-sections.

This paper is organized as follows. Section 2 is devoted to the systematic exposition of the physical foundations of the strong channel coupling (SCC) and  $R$ -matrix methods, as well as their modifications that are based on the application of nonorthogonal orbitals and  $B$ -splines as basic functions. In section 3, after a brief description of the computational scheme of the BSR version of the  $R$ -matrix method, the main techniques are discussed that are used to study  $e + \text{Ca}$  scattering resonances in the framework of the above-mentioned concept of “resonance and nonresonance channel spaces” [27–31]. There we also analyze the resonance structure in the energy dependences of the angle-integrated total cross-sections of elastic  $e + \text{Ca}$  scattering and electron-impact excitation of the  $4s4p\ ^3P^o$ ,  $3d4s\ ^3D^e$ ,  $3d4s\ ^1D^e$ ,  $4s4p\ ^1P^o$ , and  $4s5s\ ^3S^e$  states of the Ca atom. The results obtained are summarized in the final section.

## 2. Methods for Calculating Electron Scattering by Atoms

A detailed description of the SCC and  $R$ -matrix methods, as well as their capabilities to study inelastic collisions of slow electrons with atoms, was given in works [6–13, 16, 17, 21–26]. Therefore, it is pertinent to confine the theoretical part of this paper to a brief description of possible improvements of those methods, which are based on the application of time-dependent non-orthogonal orbitals and  $B$ -splines as basic functions.

### 2.1. Strong channel coupling method

In this subsection, the multichannel quantum problem of slow-electron scattering at complex atoms is considered in the framework of the SCC method. In the framework of the  $LS$ -coupling scheme, a state of the  $e + A$  system is characterized by a set of quantum numbers  $\Gamma \equiv \{\gamma, L, S, M_L, M_S, \pi\}$ , where  $L$  and  $S$  are the total orbital and spin moments, respectively;  $M_L$  and  $M_S$  are their projections on a given axis;  $\pi$  is the parity of the whole  $(N + 1)$ -electron system; and  $\gamma \equiv \{L_i, S_i, M_{L_i}, M_{S_i}, \pi_i\}$  is a similar set of quantum numbers for the target A in the  $i$ -th state. The wave function  $\Psi_\alpha^\Gamma(X, x_{N+1})$  describing the scattering of an electron by the  $N$ -electron target A is a solution of the Schrödinger equation (the atomic units  $e = m_e = \hbar = 1$  are used)

$$(H_{N+1} - E)\Psi_\alpha^\Gamma(X, x_{N+1}) = 0,$$

$$H_{N+1} = \sum_{i=1}^{N+1} \left( -\frac{1}{2} \nabla_i^2 - \frac{Z}{r_i} \right) + \sum_{i>j=1}^{N+1} \frac{1}{r_{ij}} \quad (1)$$

with certain boundary conditions for the  $e + A$  scattering problem. Here,  $r_{ij}$  is the distance between the  $i$ -th and  $j$ -th electrons,  $r_i$  is the distance from the  $i$ -th electron to the nucleus,  $H_{N+1}$  is the Hamiltonian of the  $(N + 1)$ -electron system “atom + incident electron”,  $N$  is the number of electrons in the target atom A,  $Z$  is the nuclear charge,  $E$  is the total energy of the  $e + A$  system,  $x_i \equiv (\mathbf{r}_i, \sigma_i)$  stands for the spatial and spin coordinates of the  $i$ -th electron, and  $X \equiv (x_1, \dots, x_N)$  denotes the set of spatial and spin coordinates of all  $N$  electrons in the target atom A. The subscript  $\alpha$  of the function  $\Psi_\alpha^\Gamma(X, x_{N+1})$  (the latter is often called the collision wave function) characterizes initial conditions and usually denotes the input scattering channel.

The collision wave function  $\Psi_\alpha^\Gamma(X, x_{N+1})$  can be expanded in the complete set of  $N$ -electron wave functions  $\Phi_i(X) \equiv \Phi_i(x_1, \dots, x_N)$  of the target A, which are eigenstates of the Hamiltonian  $H_N$ . The coefficients of such an expansion play the role of the wave function of incident electron. In practical calculations, this expansion is written as follows:

$$\Psi_\alpha^\Gamma(X, x_{N+1}) = A \sum_{i=1}^n \bar{\Phi}_i^\Gamma(X; \mathbf{r}_{N+1}, \sigma_{N+1}) \times \frac{F_{i\alpha}^\Gamma(r_{N+1})}{r_{N+1}} + \sum_{j=1}^m c_j \chi_j^\Gamma(X, x_{N+1}). \quad (2)$$

Here,  $A$  is the antisymmetrizing operator,  $n$  the number of channels,  $m$  the number of correlation functions  $\chi_j^\Gamma$  included into the second sum in expansion (2), and  $F_{i\alpha}^\Gamma(r)$  is the radial wave function of scattered electron in the  $i$ -th channel. The subscript  $\alpha$  characterizes the initial conditions and usually marks the input scattering channel. In practice, as a rule, expansion (2) includes all terms corresponding to open channels and only a finite number of terms describing energy-closed channels.

Let  $k_i$ ,  $l_i$ ,  $m_{l_i}$ , and  $m_{s_i}$  denote the quantum numbers of incident electron. The channel wave functions  $\bar{\Phi}_i^\Gamma$  contain the atomic wave functions  $\Phi_i(x_1, \dots, x_N)$ , as well as the spin,  $\chi_{\frac{1}{2}m_{s_i}}$ , and angular,  $Y_{l_i m_{l_i}}$ , parts of the wave function of the incident electron, which are mutually related according to the addition rules of moment vectors. In the case of nonrelativistic Hamiltonian  $H_{N+1}$ , this relation corresponds to the fixed values of the total orbital momentum  $L$  and the total spin  $S$ , with each of those quantities commuting with the Hamiltonian  $H_{N+1}$ . Then, the expansion of the channel function  $\bar{\Phi}_i^\Gamma$  in the target states  $\Phi_i$  looks like

$$\begin{aligned} & \bar{\Phi}_i^\Gamma(x_1, \dots, x_N; \hat{\mathbf{r}}_{N+1}, \sigma_{N+1}) = \\ & = \sum_{M_{L_i} m_{l_i}} \sum_{M_{S_i} m_{s_i}} (L_i M_{L_i}, l_i m_{l_i} | L M_L) \times \\ & \times (S_i M_{S_i}, \frac{1}{2} m_{s_i} | S M_S) \Phi_i(x_1, \dots, x_N) \times \\ & \times Y_{l_i m_{l_i}}(\hat{\mathbf{r}}_{N+1}) \chi_{\frac{1}{2} m_{s_i}}(\sigma_{N+1}), \end{aligned} \quad (3)$$

where the standard notation for the Clebsch–Gordan coefficients is used.

The wave function of the continuum,  $F_{i\alpha}^\Gamma(r)$ , which describes the radial motion of scattered electron in the  $i$ -th channel, is defined as follows:

$$F_{i\alpha}^\Gamma(r) \equiv F_{k_i l_i \alpha}^\Gamma(r), \quad F_{i\alpha}^\Gamma(0) = 0, \quad \varepsilon_i = k_i^2/2. \quad (4)$$

The total energy of the  $(N+1)$ -electron system equals  $E = E_i(Z, N) + \varepsilon_i$ , where  $E_i(Z, N)$  is the energy of the atomic state corresponding to the  $i$ -th channel, and  $\varepsilon_i = k_i^2/2$  is the kinetic energy of the incident electron (in atomic units). If the difference  $E - E_i$  is positive, which corresponds to the open channel, then the continuum function  $F_{i\alpha}^\Gamma(r)$  includes a divergent wave at infinity; otherwise, i.e., if  $E - E_i < 0$ , the function  $F_{i\alpha}^\Gamma(r)$  is quadratically integrable.

The total wave function (2) of the  $(N+1)$ -electron system is expanded in the set of target states and pseudostates, the wave functions  $\Phi_i(X)$  of which are constructed as linear combinations

$$\Phi_i(X) = \sum_j c_{ij} \varphi_j(x_1, \dots, x_N), \quad (5)$$

where  $\varphi_j$  is a given set of antisymmetric single-configuration functions corresponding to a certain target state  $\{L_i, S_i, \pi_i\}$ . The energy spectrum  $E_i(Z, N)$  of target A and the expansion coefficients  $c_{ij}$  can be determined from the diagonalization condition for the  $N$ -electron Hamiltonian  $H_N$  in the basis of functions (5),

$$\langle \Phi_i | H_N | \Phi_j \rangle = E_i(Z, N) \delta_{ij}. \quad (6)$$

In the framework of the multi-configuration Hartree–Fock (MCHF) method, the configuration state functions (CSFs)  $\varphi_j(x_1, \dots, x_N)$  can be expressed as the antisymmetric product of single-electron wave functions  $\varphi_{\alpha_j}(x_j)$ . If the spin-orbit interaction is insignificant, the wave function of a separate electron in the central field can be represented as the product of the spatial and spin functions,

$$\begin{aligned} \varphi_{\alpha_j}(x) & = \varphi_{n_j l_j m_j}(\mathbf{r}) \chi(m_s | \sigma) = \\ & = \frac{1}{r} P_{n_j l_j}(r) Y_{l_j m_j}(\hat{\mathbf{r}}) \chi(m_s | \sigma), \end{aligned} \quad (7)$$

where  $n_j$ ,  $l_j$ , and  $m_j$  are the principal, azimuthal, and magnetic quantum numbers, respectively;  $m_s$  is the spin projection; and  $\alpha_j$  denotes the set of quantum numbers  $\{n_j, l_j, m_j, m_s\}$ . The fundamental issue is the selection of the type of radial single-electron wave functions  $P_{n_j l_j}(r)$  – they can be analytical orbitals of the Slater type, or Hartree–Fock orbitals in a self-consistent field, or radial orbitals  $P_{n_j l_j}(r)$  in simple static model potentials – and the configurations included in expansion (5) of target states and pseudostates. The program codes allowing the calculation

of those orbitals and atomic states were carefully described in our previous works [6, 9, 11, 13, 21]. Here, we only note that the solutions of matrix equation (6) determine the eigenvalues of the target atom energy.

The second sum on the right-hand side of expansion (2) contains the quadratically integrable correlation functions  $\chi_j^\Gamma(X, x_{N+1})$ , which describe the bound states in the  $(N+1)$ -electron system and possess the same angular symmetry as  $\Psi_\alpha^\Gamma(X, x_{N+1})$ . These functions serve to improve the description of the system states at small distances from the nucleus and often lead to a faster convergence of expansion (2). Making use of the functions  $\chi_j^\Gamma$ , it is also possible to take into account the effect of some ADSs of the negative ion  $A^-$ , which manifest themselves in the scattering of electrons at neutral atoms  $A$ . In practical calculations, the correlation functions  $\chi_j^\Gamma$  are most often used to eliminate restrictions imposed on the collision wave function  $\Psi_\alpha^\Gamma$  by the condition of the function  $F_{i\alpha}^\Gamma$  orthogonality to every radial target orbital  $P_{n_j l_j}$  with the same symmetry [16, 17],

$$\langle P_{n_j l_j} | F_{i\alpha}^\Gamma \rangle = \int_0^\infty P_{n_j l_j}(r) F_{i\alpha}^\Gamma(r) dr = 0, \text{ at } l_i = l_j. \quad (8)$$

Of course, the orthogonality condition (8) is a purely “technical” assumption because the radial orbitals  $P_{n_j l_j}$  and  $F_{i\alpha}^\Gamma$  are calculated for different potentials. This condition does not follow from the basic requirements of quantum mechanics and was introduced in the SCC method proceeding from the reasons of calculation convenience. As a result of constraints imposed on the collision function  $\Psi_\alpha^\Gamma$  by the orthogonality condition (8), the incident electron cannot be virtually captured in one of the unfilled subshells participating in expansion (5) of the target states and pseudostates. In the framework of the standard SCC method, the possibility of such a capture, as was marked above, is taken into consideration by including special additional correlation functions  $\chi_j^\Gamma$  into expansion (2). However, this method of making allowance for resonance effects is not the most advantageous one and often leads to the appearance of a nonphysical pseudoresonance structure in scattering cross-sections, as well as to the necessity to solve a cumbersome system of coupled integro-differential equations for  $F_{i\alpha}^\Gamma$ . In order to avoid these difficulties, increase the accuracy of the theory, and extend the scope of its application, we must abandon

the “forced” condition (8) of orthogonality between the continuum functions  $F_{i\alpha}^\Gamma$  and the radial target orbitals  $P_{n_j l_j}$ . Now, there is no need to separately introduce a special set of correlation functions  $\chi_j^\Gamma$ , which would account for the influence of some autoionization states, into the second sum in expansion (2) because the first sum in this expansion will already contain the wave functions of those states.

Substituting the collision function  $\Psi_\alpha^\Gamma$  in form (2) into the Schrödinger equation (1) and projecting the result in turn onto the target wave functions  $\Phi_i$  and the correlation functions  $\chi_j^\Gamma$ , we obtain a system of coupled integro-differential equations for the radial functions  $F_i \equiv F_{i\alpha}^\Gamma(r)$ ,

$$\left( \frac{d^2}{dr^2} - \frac{l_i(l_i+1)}{r^2} + \frac{2Z}{r} + k_i^2 \right) F_i(r) = 2 \sum_j (V_{ij} + W_{ij} + X_{ij}) F_j(r). \quad (9)$$

Here,  $k_i^2 = 2[E - E_i(Z, N)]$  and  $V_{ij}$  is the direct local potential, whereas the integral operators of nonlocal exchange,  $W_{ij}$ , and nonlocal correlation,  $X_{ij}$ , potentials are determined as follows:

$$\begin{aligned} W_{ij} F_j &= \int_0^\infty W_{ij}(r, r') F_j(r') dr', \\ X_{ij} F_j &= \int_0^\infty X_{ij}(r, r') F_j(r') dr'. \end{aligned} \quad (10)$$

The general expressions for the operators  $V_{ij}$ ,  $W_{ij}$ , and  $X_{ij}$  are very cumbersome. Their explicit expressions were written only for electron scattering at simple atoms. However, for complex atoms and ions, they can be constructed with the help of program code [32].

## 2.2. R-matrix method and its modifications

Let us describe the basics of the standard  $R$ -matrix method, in which the problem of Hamiltonian diagonalization in the space of both open and closed channels is reduced, in essence, to solving a system of algebraic equations. A distinctive feature of the  $R$ -matrix method consists in that the whole configuration space of the  $(N+1)$ -electron system “atom + incident electron” is divided into two regions: the inner region,  $r \leq a$ , where all particles of the system (the electrons and the nucleus) are close in pair to one another and

strongly interact, and the outer region,  $r > a$ , where the scattered electron is “sensitive” only to the local potential of its interaction with the atom. The radius  $a$  of the inner region is chosen to be minimum but such that all radial wave functions  $P_{n_j l_j}$  of atomic electrons would vanish with a given accuracy at  $r > a$ .

In the framework of this method, the  $R$ -matrix is calculated. It is determined from the equation

$$F_i^\Gamma(a) = \sum_{j=1}^n R_{ij}^\Gamma(E) \left( a \frac{dF_j^\Gamma}{dr_{N+1}} - b_j F_j^\Gamma \right)_{r_{N+1}=a}, \quad (11)$$

$i = 1, \dots, n$

by solving the problem of  $e + A$  collision in the inner region ( $r \leq a$ ). Here,  $F_j$  and  $dF_j/dr_{N+1}$  are the solutions of the system of equations (9) at the boundary  $r = a$ , and the parameters  $b_j$  can be chosen arbitrarily.

Let us solve the problem of  $e + A$  collision in the inner region. For this purpose, we express the total wave function of the  $(N + 1)$ -electron system corresponding to a given energy  $E$  in the expansion form

$$\Psi_E^\Gamma = \sum_k A_{Ek}^\Gamma \Psi_k^\Gamma. \quad (12)$$

Similarly to Eq. (2), we construct an energy-independent discrete basis of  $(N + 1)$ -electron functions for each set of quantum numbers  $\{L, S, \pi\}$ ,

$$\begin{aligned} \Psi_k^\Gamma(X, x_{N+1}) &= \\ &= A \sum_{i,j} \bar{\Phi}_i^\Gamma(X, \hat{r}_{N+1}, \sigma_{N+1}) \frac{u_j(r_{N+1})}{r_{N+1}} c_{ijk}^\Gamma + \\ &+ \sum_i \chi_i^\Gamma(X, x_{N+1}) d_{ik}^\Gamma, \end{aligned} \quad (13)$$

where the functions  $\bar{\Phi}_i^\Gamma$  and  $\chi_i^\Gamma$  have the same meaning as in expansion (2). Note now that in the first sum in the right-hand side of Eq. (13), the radial orbitals of scattered electron,  $F_{i\alpha}^\Gamma$ , were expanded in the set of basis functions  $u_j$ , which are determined within a finite interval  $0 \leq r \leq a$  and satisfy the following boundary conditions:

$$u_j(0) = 0, \quad a \frac{du_j}{dr} \Big|_{r=a} = bu_j(a), \quad (14)$$

where  $b$  is an arbitrary real constant. For the basis functions  $u_j$  satisfying the boundary conditions (14),

the Hamiltonian  $H_{N+1}$  is not Hermitian in the inner region because the surface terms do not vanish at  $r = a$ . However, these members can be removed using the Bloch operator [33]

$$L_{N+1} \equiv \sum_{i=1}^{N+1} \frac{1}{2} \delta(r_i - a) \left( \frac{d}{dr_i} - \frac{b-1}{r_i} \right). \quad (15)$$

Now, it is expedient to rewrite the Schrödinger equation (1) in the form

$$(H_{N+1} + L_{N+1} - E)\Psi = L_{N+1}\Psi. \quad (16)$$

Using the expansion of Green’s function  $(H_{N+1} + L_{N+1} - E)^{-1}$  of the operator in the left hand side of Eq. (16) in the discrete basis  $\Psi_k^\Gamma$ , the formal solution of the Schrödinger equation (1) can be written as follows:

$$|\Psi^\Gamma\rangle = \sum_k |\Psi_k^\Gamma\rangle \frac{1}{E_k^\Gamma - E} \langle \Psi_k^\Gamma | L_{N+1} | \Psi^\Gamma \rangle_{\text{int}}. \quad (17)$$

The coefficients  $c_{ijk}^\Gamma$  and  $d_{ik}^\Gamma$  in expansion (13) are determined simultaneously with the energy eigenvalues  $E_k^\Gamma$  when numerically diagonalizing the matrix of the modified Hamiltonian  $H_{N+1} + L_{N+1}$  in the discrete basis  $\Psi_k^\Gamma$  (13):

$$\langle \Psi_k^\Gamma | H_{N+1} + L_{N+1} | \Psi_{k'}^\Gamma \rangle_{\text{int}} = E_k^\Gamma \langle \Psi_k^\Gamma | \Psi_{k'}^\Gamma \rangle_{\text{int}}. \quad (18)$$

Here, the integration over the radial variables is confined to the inner  $R$ -matrix region. Since the boundary conditions (14) are imposed on the basis functions  $u_j$ , the  $E_k^\Gamma$  spectrum is discrete. The calculated eigenvalues  $E_k^\Gamma$  of the Hermitian matrix  $\langle \Psi_k^\Gamma | H_{N+1} + L_{N+1} | \Psi_{k'}^\Gamma \rangle$  are real and form a discretized continuum.

The essence of the method aimed at the discretization of the continuum of the  $(N + 1)$ -electron system “atom + incident electron”, which was proposed in our works [6–13, 21–26], consists in the expansion of the target bound orbitals  $P_{n_j l_j}(r)$  and the scattered electron orbitals  $F_{i\alpha}^\Gamma(r)$  ( $r$ ) in a complete finite set  $\{B_i\}_{i=1}^n$  of the basis splines  $B_i$  and the following single diagonalization of the matrix of the self-conjugated system Hamiltonian  $H_{N+1} + L_{N+1}$  in the discrete basis (13). The main advantage of this method of continuum discretization is based on the fact that the matrix of the total Hamiltonian  $H_{N+1} + L_{N+1}$  has a very sparse – namely, band –

structure in the  $B$ -spline basis, which considerably simplifies the solution of the corresponding system of algebraic equations. At the same time,  $B$ -splines are best suited for developing the computational methods in the scattering theory. The calculation of the matrix of the Hamiltonian  $H_{N+1} + L_{N+1}$  in the discrete basis (13) and its diagonalization can be performed using the program code [32, 34] for each fixed set of quantum numbers  $\{L, S, \pi\}$ .

By projecting Eq. (17) onto the channel functions  $\bar{\Phi}_i^\Gamma$  and carrying out calculations at the point  $r = a$ , we arrive at formula (11) in which the elements of  $R$ -matrix are determined by the expression

$$R_{ij}^\Gamma(E) = \frac{1}{2a} \sum_k \frac{w_{ik}^\Gamma(a) w_{jk}^\Gamma(a)}{E_k^\Gamma - E}. \quad (19)$$

To make expressions in formulas (11) and (19) shorter, the following notations were introduced for the exposed radial wave functions  $F_i^\Gamma$  and surface amplitudes  $w_{ik}^\Gamma$ :

$$\begin{aligned} F_i^\Gamma(r_{N+1}) &= r_{N+1} \langle \bar{\Phi}_i^\Gamma | \Psi_k^\Gamma \rangle', \\ w_{ik}^\Gamma &= a \langle \bar{\Phi}_i^\Gamma | \Psi_k^\Gamma \rangle'_{r_{N+1}=a}. \end{aligned} \quad (20)$$

The primed matrix components  $\langle \bar{\Phi}_i^\Gamma | \Psi_k^\Gamma \rangle'$  in expressions (20) mean that integration should be performed over the spatial and spin coordinates of all electrons except for the radial coordinate  $r_{N+1}$  of the scattered electron.

The formulas obtained for the  $R$ -matrix [Eq. (19)] and the continuous spectrum orbitals [Eq. (11)] describe the process of electron scattering by atoms or ions in the inner  $R$ -matrix region. Together with the expression for the coefficients  $A_{Ek}^\Gamma$  in expansion (12),

$$\begin{aligned} A_{Ek}^\Gamma &= \frac{1}{2a} (E_k^\Gamma - E)^{-1} \sum_i w_{ik}(a) \left( a \frac{dF_i^\Gamma}{dr} - b F_i^\Gamma \right)_{r=a} = \\ &= \frac{1}{2a} (E_k^\Gamma - E)^{-1} \mathbf{w}^T \mathbf{R}^{-1} \mathbf{F}^\Gamma, \end{aligned} \quad (21)$$

they allow the collision wave function  $\Psi_E^\Gamma$  to be calculated in the inner region for any total system energy  $E$ . Using relationships (11) and (19)–(21), it is possible to correctly determine the  $K$ - and  $S$ -matrices using the procedure of matching the solutions in the inner region with the asymptotic solutions in the outer region,

$$F_{i\alpha}(r) \underset{r \rightarrow \infty}{\sim} k_i^{-1/2} [\delta_{i\alpha} \sin \xi_i(r) + K_{i\alpha} \cos \xi_i(r)]. \quad (22)$$

Here,  $K_{i\alpha}$  are the elements of  $K$ -matrix,

$$\xi_i(r) = k_i r - l_i \pi / 2 + \eta_i \ln(2k_i r) + \arg \Gamma(l_i + 1 - i\eta_i) \quad (23)$$

is the asymptotic phase of the regular Coulomb function with  $\eta_i = -(Z - N)/k_i$ , and  $\arg \Gamma(l_i + 1 - i\eta_i)$  is the phase of the  $\Gamma$ -function of the complex argument. The details of matching procedure were carefully described in our papers [6, 32, 34]. The scattering  $n \times n$ -matrix  $S_{i\alpha}$  and the transition  $n \times n$ -matrix  $T_{i\alpha}$  can be determined using the known matrix relations

$$\mathbf{S} = \mathbf{1} + \mathbf{T} = \frac{\mathbf{1} + i\mathbf{K}}{\mathbf{1} - i\mathbf{K}}. \quad (24)$$

In what follows, these matrices are used to calculate the scattering cross-sections and all other observed quantities.

It is worth noting here that for the  $e + A$  scattering processes with the participation of quasi-stationary AISs, there are still no standard recipes for constructing a physically acceptable basis  $\Psi_k^\Gamma$  for the expansion of the collision wave function  $\Psi_E^\Gamma$ . Since the first sum in formula (13) does not include some channels, the results of  $R$ -matrix calculations of the electron scattering processes by atoms or ions can be considered valid only in the case where these channels are closed and the influence of the corresponding AISs is small. For this reason, the interval of collision energies where expansions (12) and (13) are applicable will be limited. An alternative approach, which was proposed in our works [6, 9, 11, 13, 21], is based on supplementing the discrete basis set  $\Psi_E^\Gamma$  with the wave functions of pseudostates that simulate the part of discrete and continuous spectra omitted in the first sum in expansion (13). This approach allows the target polarization in the field of incident electron to be taken into account rather accurately, which is especially important at low collision energies.

While performing specific numerical calculations for  $e + A$  scattering processes, the computing time is mostly spent on the calculation of the matrix elements in Eq. (18) and the diagonalization of the self-conjugate Hamiltonian  $H_{N+1} + L_{N+1}$  in the discrete basis  $\Psi_k^\Gamma$  (13). However, this time-consuming procedure has to be executed only once. Afterwards, the  $R$ -matrix can be determined within the whole energy interval using formula (19). The energy dependence of  $R$ -matrix is only governed by the energy denominator in formula (19). This circumstance allows detailed

calculations to be performed in a wide energy interval with a small energy increment. We also obtain the possibility to practically move into the complex energy plane in order to calculate the  $R$ -matrix poles and so forth.

As a rule, the choice between representations (12) and (13) for the collision wave function  $\Psi_E^\Gamma$  is associated with the convergence, stability, and accuracy of calculations. The accuracy of results largely depends on the choice of basis functions  $u_j$ . The analysis of the basic equations of the  $R$ -matrix theory, which was carried out in our works [6–13], showed that the main difficulties of this method (in particular, the weak convergence of expansion (12)) can be avoided if, instead of the basis of numerical functions  $u_j$ , the basis splines  $B_i$  with compact carriers in the inner region  $r \leq a$  are used. In practical calculations, the application of  $B$ -splines as the basis functions  $u_j$  considerably speeds up the computational process and, at the same time, provides a required accuracy of wave function approximation by splines. In such a way, it is possible to avoid the necessity to introduce the so-called Buttler corrections [35] into the diagonal matrix elements (19).

The basis splines  $B_i$  possess some properties that seem to be specially aimed at resolving computational difficulties in the  $R$ -matrix method. The idea of using the basis splines  $B_i$  in the  $R$ -matrix theory is associated with several important points. First, the finite properties of  $B$ -splines form the mathematical basis of their usage as the basis functions  $u_j$ . Namely, every  $B$ -spline has an unambiguously defined minimum compact carrier associated with the  $R$ -matrix segment  $[0, a]$ . This fact is very important for the correct formulation of scattering problem in the inner region  $0 \leq r \leq a$ . Second, the application of  $B$ -splines as the basis functions  $u_j$  is analogous to the solution of the  $e + A$  scattering problem on the  $R$ -matrix segment  $[0, a]$ , beyond which the basis splines  $B_i$  vanish. In this case, all interaction potentials, including the direct,  $V_{ij}$ , exchange,  $W_{ij}$ , and correlation,  $X_{ij}$ , ones, are projected onto the complete  $B$ -spline basis so that they become efficiently truncated in a natural way at  $r > a$ . Finally, a finite set of  $B$ -splines forms a complete basis on the segment  $[0, a]$ . This property makes it possible to construct optimal compact expansions for the radial orbitals of scattered electron,  $F_{i\alpha}^\Gamma$ , in the form of finite sums. In turn, this circumstance means that spline representations for various

quantum-mechanical operators have a highly sparse band structure, which significantly simplifies the computational scheme of the  $R$ -matrix method.

Hence, the essence of the above-described BSR version of the  $R$ -matrix method is as follows:

- the continuum radial functions  $F_{i\alpha}^\Gamma(r)$  are not orthogonalized to the target orbitals  $P_{n_j l_j}(r)$ ,
- term-dependent non-orthogonal orbitals and spline representations are used for the basis functions,
- resonance effects are considered not taking the correlation functions  $\chi_i^\Gamma$  into account.

As a result, the proposed BSR version of the  $R$ -matrix method can be applied without engaging any correlation functions  $\chi_i^\Gamma$ . Alternatively, a minimum necessary set of such functions can be used to provide the completeness of the  $R$ -matrix expansion (13). Such an approach is based on correct calculations of the continuum radial functions  $F_{i\alpha}^\Gamma(r)$  in the inner region  $r \leq a$ . The application of nonorthogonal (to the bound target orbitals  $P_{n_j l_j}(r)$ ) continuum wave functions  $F_{i\alpha}^\Gamma$  eliminates the necessity to introduce an additional set of correlation functions into the second sum in expansion (13). This operation, as was noted above, often leads to various artificial effects, e.g., pseudoresonances, which are observed in the calculation results obtained for scattering cross-sections.

Unlike the standard  $R$ -matrix method [16, 17], in the framework of its proposed BSR version [6–13, 21–26], the radial target orbitals  $P_{n_j l_j}$  are optimized for every term independently. The application of term-dependent nonorthogonal orbitals provides a more accurate description of the target states and makes it possible to most comprehensively take into account such important physical effects as the valent and covalent correlations in atoms with unfilled shells and the relaxation of the quantum-mechanical orbit of excited electron. Much in the development of the concept of non-orthogonal orbitals and the establishment of their role in the calculations of atomic structures and scattering processes was done in work [6], which served as the basis for creating the corresponding software package [32].

### 3. Resonances at Electron Scattering by Calcium Atom

The calculations of the target structure and the collision processes were carried out in this work simi-

larly to our previous calculations of electron scattering by the neutral calcium atom at low collision energies [6, 8, 36]. The total wave function  $\Psi_{\alpha}^{\Gamma}(X, x_{N+1})$  of the  $(N+1)$ -electron system “atom + incident electron” for every combination  $\Gamma \equiv \{\gamma, L, S, M_L, M_S, \pi\}$  was expanded in the set of 39 lowest spectroscopic states of the Ca atom up to the  $4s8s\ ^1S$  state. Accurate representations of the target wave functions were obtained using the MCHF method with nonorthogonal orbitals and spline representations for the basis functions [37] in the *ab initio* calculations of the Ca atomic structure. In so doing, the valent and covalent correlations were taken into account by including special additional electronic configurations with the excited core into the target state and pseudostate expansion (5). In our previous work [6], in order to find the calculation accuracy of the target wave functions, we determined the binding energies for 39 lowest spectroscopic states of Ca atom and the oscillator strengths for most important transitions in it. The accuracy of calculated binding energies turned out close to that reached in extensive MCHF calculations [38], and this description of target structure is substantially better as compared to those used in previous calculations via the standard *R*-matrix method [39–41]. The deviations of the calculated energy values from the NIST-recommended ones was, in general, less than 0.1 eV. The results of oscillator strength calculations are also in good agreement with the NIST-recommended data [43].

In this work, the BSR software package [32] was used to describe the e-Ca scattering. The specificity of its application to e+Ca scattering was described in works [6, 7]. Here, we only note that term-dependent orthogonal orbitals are used which are optimized separately for various examined states. Besides that, both the bound target orbitals and the scattered electron ones are represented in the form of expansion in the basis splines  $B_j$  determined within the finite *R*-matrix interval  $0 \leq r \leq a$ . In the calculations of e+Ca scattering, as well as in the calculations of the target bound states, we used 118 basis splines of the 8th order. The *R*-matrix radius was equal to  $a = 80a_0$ , where  $a_0 = 0.529 \times 10^{-10}$  m is the Bohr radius.

Let us proceed directly to the study of resonance phenomena at the collision of slow electrons with Ca atoms. When electrons collide with neutral atoms, the effects of virtual capture of the incident electron in the unfilled subshells of the target lead to char-

acteristic features in the elastic scattering and excitation cross-sections near the thresholds of new energetically closed channels. It can be explained as a result of the following circumstance. Along with the direct potential excitation, there exists a resonant excitation associated with the formation and decay of quasi-stationary states in the “atom + incident electron” system. The autoionization decay of such states of a negative ion  $A^-$  gives an additional contribution to the atomic excitation or elastic scattering cross-section.

It is known that most of real resonances manifest themselves in multichannel systems of electron-atom interactions. However, a lot of essential features of resonance phenomenon reveal themselves in the simpler single-channel situation. That is why we begin to discuss resonances from the single-channel case.

Let us firstly consider the properties of the partial resonant amplitude. They form a basis for tests that are often used to detect unstable quasi-stationary states (resonances) at purely elastic  $e + A$  scattering and in the absence of nonresonant background. If the point concerns the  $e + A$  collision at energies close to resonance, then the partial nonresonant waves are relatively small and the main contribution to the total scattering cross-section is given by the partial resonant wave only. As a result, a drastically pronounced and approximately symmetric maximum will be observed in the experimentally measured cross-section. Its presence, generally speaking, testifies that a certain resonance may exist.

In practice, when detecting resonances by means of phase analysis, the phase shifts  $\delta_l$  or the real and imaginary parts of the partial amplitude are determined at various energies. For the resonant amplitude, the phase shift  $\delta_{l_r}$ , corresponding to the angular momentum  $l_r$  is given by the expression [44]

$$\delta_{l_r} = \text{arctg} \left[ \frac{\Gamma}{2(E_r - E)} \right]. \quad (25)$$

As a result, at the resonance point ( $E = E_r$ ), the phase shift  $\delta_{l_r}$  equals  $\pi/2$ , the partial amplitude becomes purely imaginary, and the scattering cross-section reaches its maximum value. The specific calculations of the resonance parameters (see below) demonstrate that the phase shift  $\delta_{l_r}$  rapidly increases by a multiple of  $\pi$  near the energy  $E = E_r$ .

As a rule, the method of detecting resonances by analyzing the change rate of partial phase shifts is

applied [44]. In the case of purely elastic scattering and neglecting the contribution of nonresonant background, the change rate of phase shift (25) can be found by calculating its derivative with respect to the energy  $E$ ,

$$\frac{d\delta_{l_r}}{dE} = \frac{\Gamma/2}{(E - E_r)^2 + (\Gamma/2)^2}. \quad (26)$$

Hence, this quantity is maximum at  $E = E_r$ , which means that a resonance should be searched for. According to formula (26), the resonance width  $\Gamma$  is related to the maximum value of the derivative  $d\delta_{l_r}/dE$  as follows:

$$\Gamma = 2 \left( \frac{d\delta_{l_r}}{dE} \Big|_{E=E_r} \right)^{-1}. \quad (27)$$

Therefore, to make a conclusion about the existence or absence of resonant states with the angular momentum  $l_r$ , it is necessary to use the tests described above. However, those tests can determine the resonant state parameters easily and unambiguously only in the very rare case where the resonances are purely elastic and the nonresonant background is absent. In the general case, resonances arise in the inelastic interaction interval and are superimposed on a nonresonant background. Therefore, those tests do not allow the resonance position and width to be determined unambiguously. Hence, the tests based on the properties of partial amplitudes of the Breit–Wigner type can only provide information, albeit important, about a necessity to perform a more detailed analysis of the energy dependence of partial cross-sections to detect the resonant behavior.

In a real case, resonant interaction is accompanied by a nonresonant background, which can be taken into account by summing up the resonant part of the phase shift  $\delta_{l_r}$  (25) with a certain constant phase  $\delta_0$ ,

$$\delta(E) = \delta_0 + \delta_{l_r} = \delta_0 + \arctg \left[ \frac{\Gamma}{2(E_r - E)} \right]. \quad (28)$$

The quantity  $\delta_{l_r}$  is called the background phase shift. Assuming the energy independence of the background, the width  $\Gamma$  of an isolated resonance can be determined by formula (27).

Thus, near the resonance energy  $E_r$ , the total phase shift  $\delta(E) = \delta_0 + \delta_{l_r}$  drastically increases from  $\delta_0$  to  $\delta_0 + \pi$ . We adopt such a rapid growth of the function  $\delta(E)$  by  $\pi$  as a definition of a resonance with the angular momentum  $l_r$ .

Before passing to the general multichannel case, note that the determination of the resonance position  $E_r$  and width  $\Gamma$  by formulas (27) and (28) is, as a rule, not difficult as far as the resonance is so narrow that the background phase shift  $\delta_0$  can be considered constant within the resonance level width in a vicinity of the energy  $E_r$ . However, for a wider resonance with a short life time, the unambiguous determination of its parameters can become a difficult task. Actually, the background phase shift  $\delta_0$  is not constant but changes (slowly) with the energy  $E$ . Therefore, the exact determination of the parameters of wide resonance requires the knowledge of the behavior of the function  $\delta_0(E)$  in an energy interval about  $\Gamma$  in width near the point  $E_r$ :  $E_r - \Gamma/2 \leq E \leq E_r + \Gamma/2$ .

Note also that the simple resonance model considered above seemingly does not consider the inelastic processes, i.e., processes at which the target becomes excited or ionized. At the same time, most resonances of negative  $A^-$  ions emerge at energies where more than one channel are open. Furthermore, those resonances often overlap one another and are located near the thresholds, which impose their own constraints on the allowable behavior of phase shifts. As time went by, it became clear that the interpretation of a wider range of resonance phenomena requires the application of a multichannel theory that would be applicable, for example, to the analysis of  $e+A$  systems with close (overlapping) resonances.

In the multichannel case, the information about resonances can be obtained by analyzing the analytical properties of  $S$ -matrix in the complex energy plane. This method is simple in principle, but it requires a large amount of computation when considering a multi-channel system with a large number of overlapping resonances. An alternative possibility of resonance research is based on the multi-channel generalization of the expression [45]

$$\Delta t = 2\hbar \frac{d\delta}{dE} \quad (29)$$

for the time delay  $\Delta t$  at single-channel scattering in comparison with the time spent on the free passage of incident particles. It is known [44, 45] that the time delay  $\Delta t$  is directly related to the  $S$ -matrix, namely,

$$\Delta t = -i\hbar \frac{d}{dE} \ln S. \quad (30)$$

This relationship can be generalized to the multichannel case by introducing the lifetime matrix [27–30]

$$Q = i\hbar S \frac{dS^\dagger}{dE} = -i\hbar \frac{dS}{dE} S^\dagger = Q^\dagger(E), \quad (31)$$

where the dag symbol denotes the Hermitian conjugation. It is easy to see that in the case of elastic scattering, where  $S = \exp(2i\delta)$ , relationships (29) and (30) are equivalent. For multi-channel scattering, the diagonal elements  $Q_{ii}$  of the  $Q$ -matrix are real-valued and have the physical meaning of the time delay averaged over all possible output channels, including the input channel  $i$ .

The  $Q$ -matrix was first introduced by Smith [46]. In the literature, it is often referred to as the time-delay matrix. From definition (31) of the  $Q$ -matrix, it is evident that the latter is Hermitian so that its eigenvalues  $q_i$  are real. The sum of eigenvalues, i.e., the trace  $\text{Tr} Q$  of the matrix  $Q$ , is related to the sum of the intrinsic phases,  $\delta(E)$ , by the formula

$$2\hbar \frac{d\delta}{dE} = \text{Tr} Q(E) \equiv \sum_i Q_{ii}(E) = \sum_i q_i(E). \quad (32)$$

Below, the channels defined by the  $Q$ -matrix eigenvectors will be called eigenchannels with respect to the  $Q$ -matrix or, briefly,  $Q$ -eigenchannels. A distinctive feature of the time-delay matrix  $Q$  consists in that for an isolated resonance with a background  $S$ -matrix independent of the energy  $E$ , only the non-zero eigenvalue has the Lorentzian form  $L(E)$  [28]. In other words, only the  $Q$ -eigenchannel corresponding to this Lorentzian eigenvalue is associated with the resonance, and all other  $Q$ -eigenchannels are independent of the resonance asymptotically.

In work [29], this result was extended to overlapping resonances. If the energy intervals of two resonances overlap and the background  $S$ -matrix is independent of  $E$ , two eigenvalues of the  $Q$ -matrix,  $\{q_i(E), i = 1, 2\}$ , have Lorentzian profiles that avoid each other only near their intersection points. Their sum is a simple sum of two Lorentzians. All other eigenvalues equal zero. This means that only two  $Q$ -eigenchannels are associated with those resonances, and all other  $Q$ -eigenchannels are not associated with the resonances asymptotically.

Finally, the theorem proved in works [30, 31] generalizes this (latter) result on the case of  $N$  overlapping resonances. Namely, only  $N$  eigenvalues of

the  $Q$ -matrix are different from nonzero and possess Lorentzian profiles that avoid each other near their intersection points, thus proving that the background  $S$ -matrix is independent of the energy  $E$ . Any of the overlapping resonances can only decay into  $N$   $Q$ -eigenchannels corresponding to those eigenvalues but none of other  $Q$ -eigenchannels. Thus, the set of  $Q$ -eigenchannels can be divided into a “resonant channel space”, i.e., a subset of  $N$   $Q$ -eigenchannels associated with the resonances, and its asymptotic complement, which is not related to the resonances and comprises a nonresonant background.

According to the theorem formulated above, in the case of more than one overlapping resonance, the single-channel Breit–Wigner formulas (26) and (28) should be replaced by the corresponding multi-channel formulas for the eigenphase sum  $\delta(E)$  and the  $Q$ -matrix trace  $\text{Tr} Q$ ,

$$\delta(E) = \sum_{\nu=1}^N \text{arctg} \frac{\Gamma_\nu/2}{E_\nu - E} + \delta_b(E), \quad (33)$$

$$\begin{aligned} \text{Tr} Q(E) &= \sum_{\nu=1}^N L_\nu(E) + 2\hbar \frac{d\delta_b(E)}{dE} \equiv \\ &\equiv \sum_{\nu=1}^N \frac{\hbar\Gamma_\nu}{(E - E_\nu)^2 + (\Gamma_\nu/2)^2} + 2\hbar \frac{d\delta_b(E)}{dE}. \end{aligned} \quad (34)$$

Here,  $E_\nu$  denotes the position and  $\Gamma_\nu$  the width of the  $\nu$ -th resonance. Now, the contribution of overlapping resonances is described by the sum of  $N$  terms, each of which has a typical resonance form [see formulas (25) and (26)]. At the same time, the summand  $\delta_b(E)$  includes the sum of the background eigenphases. As a result, the trace  $\text{Tr} Q(E)$  of the  $Q$ -matrix is a simple superposition of the Lorentzian curves  $L_\nu(E)$ , except for the usually small nonresonant background. Assuming that only one eigenphase is important at energies in a vicinity of  $E_\nu = E_r$ , i.e., the resonance is isolated, we may neglect summation in relationship (33) to obtain formula (28) for single-channel scattering.

If the above-described concept of the “space of resonant channels” is applied to e+Ca collision processes, the following points can be clearly distinguished.

1. Resonance states can decay into any open channel of common symmetry. They can also decay into any of their eigenchannels determined by the  $S$ -matrix diagonalization. However, it is known that an isolated resonance can only decay into one (separate)

of its eigenchannels, which is determined by the diagonalization of the time-delay matrix (31). This selected  $Q$ -eigenchannel is associated with an eigenvalue, the dependence of which on the energy  $E$  has the Lorentzian form  $L_\nu(E)$ .

**Table 1. Possible terms of the odd states of  $\text{Ca}^-$  ion in the energy interval up to about 4.3 eV**

Configuration	Possible terms	Number	
		a	b
$4s4p[{}^3P]3d$	$4.2P, 4.2D, 4.2F^o$	6	6
$4s3d[{}^3D]4p$	$4.2P, 4.2D, 4.2F^o$	6	4
$4s3d[{}^1D]4p$	$2P, 2D, 2F^o$	3	2
$4s4p[{}^1P]3d$	$2P, 2D, 2F^o$	3	3
$4s4p[{}^1P]4d$	$2P, 2D, 2F^o$	3	1
$4s5s[{}^3S]5p$	$4.2P^o$	2	2
$4s5s[{}^3S]6p$	$4.2P^o$	2	2
$4s5s[{}^3S]4f$	$4.2F^o$	2	2
$4s5s[{}^1S]5p$	$2P^o$	1	1
$4s5s[{}^1S]4f$	$2F^o$	1	1
Total		29	24

a – the number of possible terms of given configuration.  
 b – the number of identified terms of given configuration.

**Table 2. Possible terms of the even states of  $\text{Ca}^-$  ion in the energy interval up to about 4.3 eV**

Configuration	Possible terms	Number	
		a	b
$4s^23d$	$2D$	1	1
$4s4p^2[{}^3P]$	$4.2P, 2D, 2S$	4	4
$4s4p[{}^3P]4f$	$4.2D, 4.2F, 4.2G$	6	5
$4s3d[{}^3D]5s$	$4.2D$	2	2
$4s3d^2$	$2S, 4.2P, 2D, 4.2F, 2G$	7	4
$4s4p[{}^1P]4f$	$2D, 2F, 2G$	3	3
$4s3d[{}^3D]4d$	$4.2S, 4.2P, 4.2D, 4.2F, 4.2G$	10	4
$4s3d[{}^1D]4d$	$2S, 2P, 2D, 2F, 2G$	5	4
$4s5s^2[{}^1S]$	$2S$	1	1
$4s5s[{}^3S]4d$	$4.2D$	2	2
$4s5s[{}^1S]6s$	$2S$	1	1
$4s5s[{}^1S]4d$	$2D$	1	1
Total		43	32

a – the number of possible terms of given configuration.  
 b – the number of identified terms of given configuration.

2. Since the incident electron can be captured by the target into any possible ADS of the negative  $\text{Ca}^-$  ion, the resonances in the spectrum of  $e + \text{Ca}$  scattering cross-sections are grouped within the energy intervals located before the opening of the next inelastic channel. This behavior allows us to express some general considerations about the decay of possible ADSs corresponding to a certain configuration of the negative  $\text{Ca}^-$  ion and approaching the excitation threshold of one of the closely located states of a Ca atom. Among other characteristics, each ADS of the negative  $\text{Ca}^-$  ion has a definite parity. The decay of such states can occur via that or another channel, with the parity being conserved. Therefore, in Tables 1 and 2, we systematized possible ADSs of the negative  $\text{Ca}^-$  ion in accordance with their parities. Those states will be the objects of our further study.

3. The eigenphases  $\delta_\alpha$  defined in this section are, in essence, the phases of the diagonal elements in the  $S$ -matrix (see work [31]). The latter is related to the  $K$ -matrix (the reactance matrix) by means of relationship (24). This relation allows the phases  $\delta_\alpha$  to be calculated in the framework of the BSR version of the  $R$ -matrix method, which was described in section 1, with the help of the RESFIT software package [47]. When analyzing the structure of resonances, this package allows the Lorentzian profile of the derivative in the interval of resonance energies to be correctly reproduced at the quantitative level. In so doing, the  $K$ -matrix is fitted to an analytical form that contains information about the resonance position and width, as well as the background  $K$ -matrix. The results of such calculations obtained for the sum  $\delta$  of eigenvalues  $\delta_\alpha$  and its energy derivative  $d\delta(E)/dE$ , as well as the positions and widths of resonances in the integral cross-section (ICS) of  $e + \text{Ca}$  scattering, are exhibited in Fig. 1 and Tables 3 to 5. Three asterisks (\*\*\*) in Tables 3 and 4 mark the most probable, i.e., reliably established in our calculations, resonances (see Table 5). For such resonances, the magnitude of the phase shift jump varies within the interval  $0.65\pi \leq \delta_\alpha \leq \pi$  when passing through the resonance point  $E = E_r$ . If the phase shift jump at the passage through the resonance point lies within the interval  $\pi/2 < \delta_\alpha < 0.65\pi$ , the corresponding possible (quite probable) resonance state of  $\text{Ca}^-$  is marked with two asterisks (\*\*). In this case, the existence of the  $\text{Ca}^-$  resonance states cannot be established without involving additional information, for instance, about

the resonant behavior of the scattering cross-section near the energy  $E = E_r$ . If the magnitude of the phase shift jump is within the interval  $0 < \delta_\alpha < \pi/2$ , then the possible  $\text{Ca}^-$  states are marked with a single asterisk (\*). In this case, there exist such states of the negative  $\text{Ca}^-$  ion that do not result in any observable resonant (physical) effect. By comparing the data in Tables 3 to 5, the conclusion can be drawn that 24 (i.e., 83%) of 29 possible (for selected configurations) odd states and 32 (i.e., 74%) of 43 possible even ones in the energy interval from the reaction threshold to 4.3 eV were confirmed in our calculations. It is the multiple character of detected resonances that leads to their noticeable contribution to the  $e + \text{Ca}$  scattering cross-section, despite that the widths of most resonances (see Tables 3 to 5) are rather small.

**Table 3. Position  $E_r$  and width  $\Gamma$  of the possible resonances of odd states in the integral cross sections of  $e + \text{Ca}$  scattering in the energy interval up to about 4.3 eV**

$E_r$ , eV	$\Gamma$ , MeV	The reliability degree of the detected resonance $\text{Ca}^-$ state	Probable classification
1.893	0,2	**	$4s4p[{}^3P]3d[{}^2P^\circ]$
1.922	40	*	$4s4p[{}^3P]3d[{}^2D^\circ]$
1.93	39	*	$4s4p[{}^3P]3d[{}^2F^\circ]$
2.121	59	***	$4s4p[{}^3P]3d[{}^4F^\circ]$
2.251	140	***	$4s3d[{}^3D]4p[{}^2D^\circ]$
2.48	128	**	$4s4p[{}^3P]3d[{}^4P^\circ]$
2.523	13	***	$4s4p[{}^3P]3d[{}^4D^\circ]$
2.532	14	**	$4s3d[{}^1D]4p[{}^2D^\circ]$
2.533	16	*	$4s3d[{}^3D]4p[{}^2F^\circ]$
2.533	18	*	$4s3d[{}^3D]4p[{}^4F^\circ]$
2.534	24	*	$4s3d[{}^3D]4p[{}^4P^\circ]$
2.719	16	**	$4s4p[{}^1P]3d[{}^2D^\circ]$
2.723	18	**	$4s3d[{}^1D]4p[{}^2F^\circ]$
2.797	116	**	$4s4p[{}^1P]3d[{}^2F^\circ]$
2.93	1	*	$4s4p[{}^1P]3d[{}^2P^\circ]$
2.967	45	*	$4s4p[{}^1P]4d[{}^2F^\circ]$
3.826	16	***	$4s5s[{}^3S]5p[{}^4P^\circ]$
3.877	7	***	$4s5s[{}^3S]5p[{}^2P^\circ]$
3.914	5	**	$4s5s[{}^3S]6p[{}^4P^\circ]$
3.967	40	**	$4s5s[{}^3S]4f[{}^2F^\circ]$
3.977	97	*	$4s5s[{}^3S]4f[{}^4F^\circ]$
4.059	42	*	$4s5s[{}^3S]6p[{}^2P^\circ]$
4.132	4	*	$4s5s[{}^1S]5p[{}^2P^\circ]$
4.201	56	**	$4s5s[{}^1S]4f[{}^2F^\circ]$

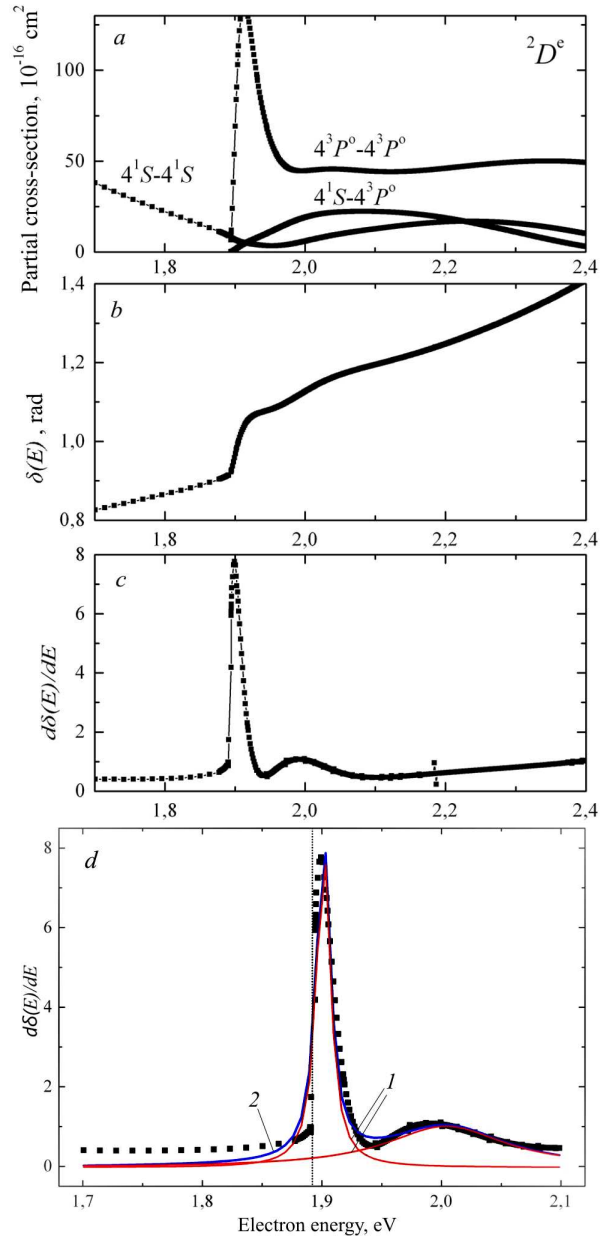


**Fig. 1.** Example of overlapping resonances at  $e + \text{Ca}$  scattering. Partial contributions of  ${}^2D^e$  wave to the integral cross-sections (ICSS) of elastic  $e + \text{Ca}$  scattering in the  $4s^2 {}^1S$  and  $4s4p {}^3P^\circ$  states of  $\text{Ca}$  atom and excitation of the  $4s^2 {}^1S - 4s4p {}^3P^\circ$  transition (a). Energy dependence of the eigenphase sum  $\delta(E)$  for the partial  ${}^2D^e$  wave (b). Energy dependence of the  $d\delta(E)/dE$  in the overlapping interval of the resonances  $4s4p[{}^3P]4f {}^2D$  and  $4s4p^2 {}^2D$  (c). Lorentzian profiles of the energy derivatives of eigenphases (curves 1) and their sum (curve 2) in the case of two overlapping resonances  $4s4p[{}^3P]4f {}^2D$  and  $4s4p^2 {}^2D$  (d)

4. For multi-electron systems of the Ca type, an essential role in  $e + \text{Ca}$  scattering is played by non-central interaction among outer (bound) Ca electrons, as well as their interaction with the incident electron. In such systems, a series of resonances with the same total angular momentum and parity are observed. They are grouped near the excitation threshold of one of closely located states of Ca atom. This is demonstrated in Tables 3 and 4, where the param-

**Table 4. Position  $E_r$  and width  $\Gamma$  of the possible resonances of even states in the integral cross sections of  $e + \text{Ca}$  scattering in the energy interval up to about 4.3 eV**

$E_r$ , eV	$\Gamma$ , MeV	The reliability degree of the detected resonance $\text{Ca}^-$ state	Probable classification
1.193	700	***	$4s^23d[{}^2D]$
1.899	12	**	$4s4p^2[{}^3P][{}^4P]$
1.899	12	**	$4s4p^2[{}^3P][{}^2P]$
1.901	14	**	$4s4p[{}^3P]4f[{}^2D]$
1.903	17	**	$4s4p[{}^3P]4f[{}^4D]$
1.957	97	*	$4s4p[{}^3P]4f[{}^4F]$
1.966	113	*	$4s4p[{}^3P]4f[{}^2F]$
1.975	65	*	$4s4p[{}^3P]4f[{}^2G]$
2.004	122	**	$4s4p^2[{}^2D]$
2.075	246	**	$4s4p^2[{}^2S]$
2.524	1	*	$4s3d[{}^3D]5s[{}^2D]$
2.524	0,3	*	$4s3d[{}^3D]5s[{}^4D]$
2.556	39	*	$4s3d^2[{}^3F][{}^4F]$
2.558	53	*	$4s3d^2[{}^3F][{}^2F]$
2.559	40	*	$4s3d^2[{}^3P][{}^2P]$
2.56	44	*	$4s3d^2[{}^1G][{}^2G]$
2.718	126	*	$4s4p[{}^1P]4f[{}^2D]$
2.743	33	*	$4s4p[{}^1P]4f[{}^2F]$
2.75	45	*	$4s4p[{}^1P]4f[{}^2G]$
2.833	256	*	$4s3d[{}^3D]4d[{}^2P]$
2.938	12	**	$4s3d[{}^1D]4d[{}^2P]$
3.018	141	*	$4s3d[{}^3D]4d[{}^2G]$
3.019	102	**	$4s3d[{}^3D]4d[{}^2F]$
3.208	1029	*	$4s3d[{}^3D]4d[{}^4F]$
3.386	369	**	$4s3d[{}^1D]4d[{}^2G]$
3.414	1462	**	$4s3d[{}^1D]4d[{}^2F]$
3.659	101	***	$4s3d^2[{}^1S][{}^2S]$
3.875	3	***	$4s5s^2[{}^1S][{}^2S]$
3.917	4	***	$4s5s[{}^3S]4d[{}^2D]$
3.928	15	**	$4s5s[{}^3S]4d[{}^4D]$
4.099	3	***	$4s5s[{}^1S]6s[{}^2S]$
4.143	11	***	$4s5s[{}^1S]4d[{}^2D]$

eters (the position  $E_r$  and the width  $\Gamma$ ) of resonances in the ICS of  $e + \text{Ca}$  scattering are quoted separately for even and odd ADSs of the negative  $\text{Ca}^-$  ion. The last column of Tables 3 to 5 contains the illustrative scheme of the classification proposed by us for the detected resonances in the interval of incident-electron energies from 1.893 to 4.3 eV. As one can see from Tables 3 to 5, the resonances are arranged very close to one another in the indicated energy interval and most of them are rather narrow.

5. Detailed calculations of  $Q$ -matrix eigenvalues determine the number  $N$  of Lorentzian profiles  $L_\nu(E)$  that must be included into formula (34) in order to accurately calculate the trace of  $Q$ -matrix. In the case of an isolated narrow resonance with a long lifetime, the sum  $\delta(E)$  of all eigenphases is well described by the one-level Breit–Wigner formula (28) and drastically increases by almost  $\pi$  in a narrow vicinity of the resonance energy  $E = E_r$ . Recently, the method of detecting resonances by measuring the change rate of partial phase shifts has been often applied [31]. It was found that the derivative  $d\delta(E)/dE$  turned out more informative for the analysis of resonance features than the eigenvalue sum  $\delta(E)$  itself. This fact has both practical and physical aspects. On the one hand, resonances can be more clearly distinguished in the derivative  $d\delta(E)/dE$  than in the eigenvalue sum  $\delta(E)$ . On the other hand, the derivative  $d\delta(E)/dE$  is directly related to the lifetime of resonance state, which allows a transparent physical interpretation to be made. In addition, the trace

**Table 5. Position  $E_r$  and width  $\Gamma$  of the reliably established resonances in the integral cross-sections of  $e + \text{Ca}$  scattering in the energy interval up to about 4.3 eV**

Energy $E_r$ , eV	Width $\Gamma$ , MeV	Phase shift, $\pi$	Classification
1.193	700	0.83	$4s^23d {}^2D$
2.121	59	0.83	$4s4p[{}^3P]3d^4F^o$
2.251	140	0.84	$4s3d[{}^3D]4p^2D^o$
2.523	13	0.85	$4s4p[{}^3P]3d^4D^o$
3.659	101	0.72	$4s3d[{}^1D]4d^2S$
3.826	16	0.9	$4s5s[{}^3S]5p^4P^o$
3.875	3	0.98	$4s5s^2 {}^2S$
3.877	7	0.96	$4s5s[{}^3S]5p^2P^o$
3.917	4	0.77	$4s5s[{}^3S]4d^2D$
4.099	3	0.86	$4s5s[{}^1S]6s^2S$
4.143	11	0.67	$4s5s[{}^1S]4d^2D$

of  $Q$ -matrix, as well as the derivative  $d\delta(E)/dE$ , has a Lorentzian profile in the interval of resonance energies, and this profile can be reproduced quantitatively by means of the OriginPro 7.0 tools. A graphic illustration of the aforesaid is presented in Fig. 1, where the main stages of the procedure aimed at analyzing the structure of resonance features in the ICS of  $e + \text{Ca}$  scattering for the  ${}^2D^e$  wave at energies of 1.901 and 2.004 eV are presented. The resonance parameters (the position  $E_\nu$  and the width  $\Gamma_\nu$ ) obtained from the analysis of the energy dependence of the derivative  $d\delta(E)/dE$  near the excitation thresholds of atomic levels are quoted in Table 3 for the odd states and in Table 4 for the even ones.

A practical conclusion from the above is as follows: early indications for the existence of resonances should be sought in the energy dependences of not only the scattering cross-sections but also the eigenphase sum  $\delta(E)$  in the vicinity of resonance energy  $E_r$ . In the general case of multi-channel scattering, more complete information concerning the resonance parameters ( $E_\nu$ ,  $\Gamma_\nu$ ) can be obtained by analyzing the derivative  $d\delta(E)/dE$  of the eigenphase sum  $\delta(E)$  with respect to the energy  $E$ . When analyzing such resonances, instead of “single-channel” Breit–Wigner formulas (26) and (28), the corresponding “multi-channel” formulas (33) and (34) should be used.

To illustrate the general provisions formulated above, we also give an example of two possible overlapping resonances located at energies of 1.901 and 2.004 eV (see Fig. 1). In particular, Fig. 1, *b* demonstrates the energy dependence of the eigenphase sum  $\delta$  (in  $\pi$  units) in the  ${}^2D^e$  wave for elastic  $e + \text{Ca}$  scattering in the  $4s^2\ ^1S$  and  $4s4p\ ^3P^o$  states and excitation of the  $4s^2\ ^1S - 4s4p\ ^3P^o$  transition. In the course of collision at energies of 1.901 and 2.004 eV, the incident electron and the Ca atom can form a quasi-bound  $\text{Ca}^-$  system in the  $4s4p[{}^3P]4f\ ^2D$  and  $4s4p^2\ ^2D$  states, respectively.

The Lorentzian profiles corresponding to the  $4s4p[{}^3P]4f\ ^2D$  and  $4s4p^2\ ^2D$  resonances, which are depicted in Fig. 1, *d* by red curves, were obtained by carrying out the Lorentzian fitting of the eigenphase derivatives in the partial  ${}^2D^e$  wave. The resonance peaks observed in those curves at energies of 1.901 and 2.004 eV (see Fig. 1, *d*) are spaced appreciably apart. The resulting dependence was obtained using the Lorentzian fitting of the energy dependence of the derivative  $d\delta(E)/dE$  of the sum of

eigenphases of two indicated resonances and is shown in Fig. 1, *d* as a blue curve. The positions and widths of the fitted Lorentzians correspond to the positions and widths of the corresponding resonances in the ICS of  $e + \text{Ca}$  scattering, which were calculated in the BSR39 approximation and are shown in Figs. 1, *a–d* by squares.

The RESFIT software package [47] was used to calculate the eigenphases  $\delta_\alpha$ . The energies of the  $4s4p[{}^3P]4f\ ^2D$  and  $4s4p^2\ ^2D$  eigenstates were calculated by diagonalizing the Hamiltonian of the  $e + \text{Ca}$  system. In the interval of collision energies from 1.892 to 2.075 eV, the eigenphase sum drastically increases, as is shown in Fig. 1, *b*. The corresponding partial  ${}^2D$  cross-sections of elastic electron scattering by the Ca atom in the metastable  $4s4p\ ^3P^o$  state and excitation of the  $4s^2\ ^1S - 4s4p\ ^3P^o$  transition reach their maximum values at energies of 1.901 and 2.004 eV, respectively (see Fig. 1, *a*). Note that in the resonance interval, the eigenphase of the  $4s4p[{}^3P]4f\ ^2D$  state passes the point  $\delta = \pi/2$  with a larger energy derivative  $d\delta(E)/dE$  than the eigenphase of the  $4s4p^2\ ^2D$  state does, which is clearly seen from Figs. 1, *c* and *d*.

#### 4. Partial and Integral Cross-Sections of Electron Scattering at Calcium Atom in the Energy Interval Below 4.3 eV

In principle, the results of sections 2 and 3 give everything necessary for a detailed analysis of the processes of slow-electron scattering (elastic and inelastic) by the Ca atom. The results of calculations obtained in the BSR approximation for the ICSs of elastic  $e + \text{Ca}$  scattering and electron-impact excitation of the  $4s4p\ ^3P^o$ ,  $3d4s\ ^3D^e$ ,  $3d4s\ ^1D^e$ ,  $4s4p\ ^1P^o$ , and  $4s5s\ ^3S^e$  states of the Ca atom in the interval of collision energies up to 4.3 eV are shown in Figs. 2 and 3. The corresponding panels also demonstrate the contributions of the partial  ${}^2S^e$ ,  ${}^2P^o$ ,  ${}^2D^e$ , and  ${}^2F^o$  waves to the ICS in the indicated processes. The vertical thin lines in the figures mark the excitation thresholds of the Ca atomic states. One can see that peculiarities of the sharpening-point type are observed near those thresholds.

As can be seen from Figs. 2, *b* and *c* and Figs. 3, *a–c*, the excitation of the  $4s4p\ ^3P^o$  state gives the main inelastic contribution to the total cross-section of  $e + \text{Ca}$  scattering at energies of 2–2.4 eV. At energies higher

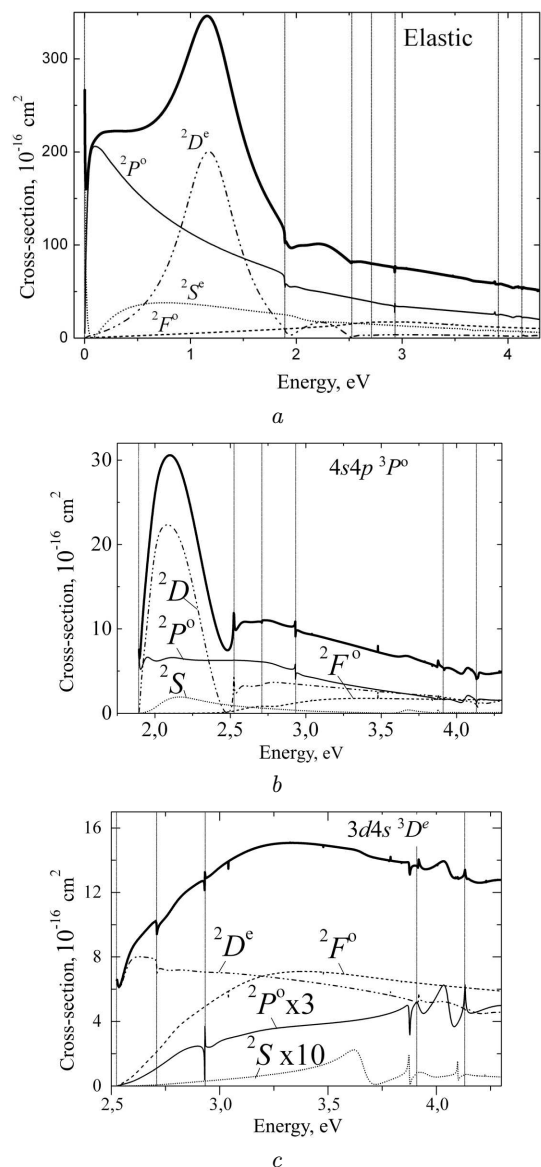


**Fig. 2.** The ICSs of elastic e + Ca scattering and excitation of the  $4s4p\ ^3P^o$  and  $3d4s\ ^3D^e$  states of Ca atom (bold solid curve). Contributions to the ICS of e + Ca scattering from the partial waves  $^2S^e$  (dotted curve),  $^2P^o$  (thin solid curve),  $^2D^e$  (dash-double-dotted curve), and  $^2F^o$  (dashed curve). Vertical thin lines mark the excitation thresholds of Ca atom

than 2.5 eV, the contribution to the ICS induced by the excitation of the  $3d4s\ ^3D^e$  state dominates, whereas the contributions from the excitation of the levels  $3d4s\ ^1D^e$  and  $4s5s\ ^3S^e$  are relatively small. Finally, at even higher energies ( $E > 4.3$  eV) – they are not shown in Figs. 2 and 3 – the main inelastic

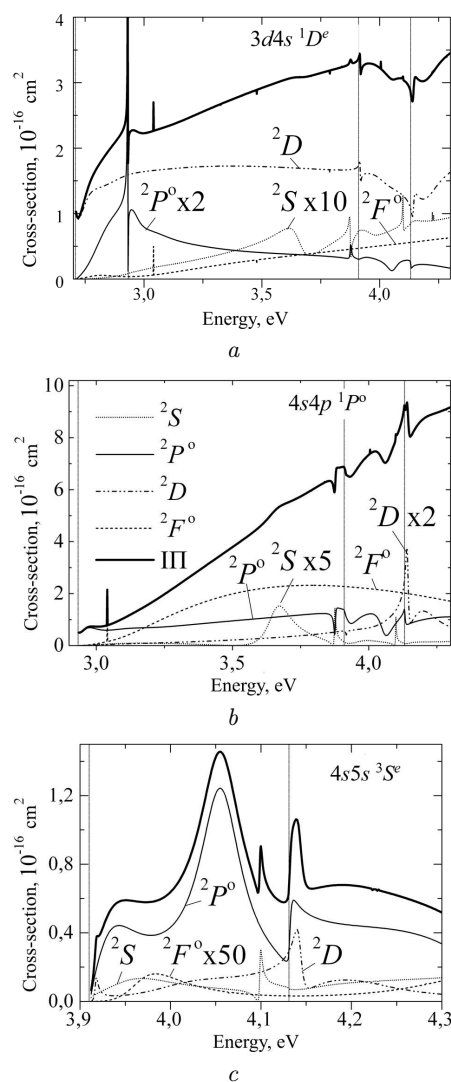


**Fig. 3.** The same as in Fig. 2 but for the ICSs of the  $3d4s\ ^1D^e$ ,  $4s4p\ ^1P^o$ , and  $4s5s\ ^3S^e$  states of Ca atom

contribution to the total cross-section is provided by strong dipole excitation of the  $4s4p\ ^1P^o$  level.

The partial  $^2S^e$ ,  $^2P^o$ ,  $^2D^e$ , and  $^2F^o$  cross-sections shown in Fig. 2, *a* make it possible to find the origin of characteristic structures in the cross-section of elastic e + Ca scattering. The smooth maxima in the  $^2S^e$  and  $^2P^o$  symmetries cannot be identified with resonances. Instead they appear due to rapid changes in the phase shifts in the *s*- and *p*-waves at low energies. The combined action of short-range exchange repulsion and long-range attraction (proportional to  $r^{-4}$  and emerging owing to the polarization of the Ca

atom in the field of incident electron) brings about the Ramsauer–Townsend effect, which has long been of interest for a number of spectroscopic applications [34, 48] and leads to a strongly nonmonotonic (i.e., irregular) dependence of the  $e + \text{Ca}$  scattering cross-section on the collision energy  $E$ . As a result, the phase shift for the  $s$ -wave passes through zero at  $E = 0.07$  eV, where just the partial  ${}^2S$  cross-section becomes responsible for the appearance of the Ramsauer–Townsend minimum in the total cross-section of elastic  $e + \text{Ca}$  scattering. However, the dominant 1.193-eV peak is obviously a result of the resonance in the partial  ${}^2D$  cross-section, which can be unambiguously identified as the  $4s^23d$   ${}^2D$  shape resonance. The phase shift in this energy interval changes by almost  $0.83\pi$ . In Fig. 2, *a*, one can also observe a small peak at higher energies between the  $4s4p$   ${}^3P^\circ$  and  $3d4s$   ${}^3D$  excitation thresholds. Yuan and Lin [40] identified this peak in the framework of the standard  $R$ -matrix method as the  $4s4p^2$   ${}^2D$  resonance. On the other hand, our results do not point to a distinct correspondence between this peak and the resonance. The phase shift in the  $d$ -wave really begins to increase in this energy interval, as it would be for a real resonance, but the  $d$ -phase begins to rapidly decrease at the  $3d4s$   ${}^3D$  threshold, thus giving a total growth of only  $\pi/4$  in the region of maximum. It seems that this possible (hypothetical) resonance is destroyed owing to the opening of new decay channels. This conclusion makes us suppose the existence of another resonance in the  $s$ -wave with the  $4s4p^2$   ${}^2S$  configuration and the parameters  $E_r = 2.075$  eV and  $\Gamma = 246$  meV (see Table 4).

Kazakov and Khristoforov [49] measured the elastic scattering differential cross-sections and the excitation functions of the  $4s4p$   ${}^3P^\circ$  and  $4s3d$   ${}^3D$  states of the Ca atom at an angle of  $90^\circ$  in the energy interval of 0–7 eV. They observed a wide resonance (maximum) in the elastic scattering cross-section near 1.25 eV, which was attributed to the  ${}^2D$  shape resonance. A narrower  $p$ -wave resonance lies at very low energies and, at an observation angle of  $90^\circ$ , looks like a minimum centered at  $E_o = 0.1$  eV. Besides the resonant features indicated above, they also found a relatively sharp feature at the  $4s4p$   ${}^3P^\circ$  threshold, which manifested itself in both the elastic cross-section and the excitation function of the  $4s4p$   ${}^3P^\circ$  level. They supposed the latter to be a result of a resonance. Their data demonstrated a broad feature at

about 3 eV, which may be related to the  $4s4p^2$   ${}^2D$  resonance. The cited authors also commented the availability of another structure in the cross-section near the  $4s5s$   ${}^3,1S$  and  $4s5p$   ${}^3P^\circ$  thresholds, but the data presented in their work [49] cannot be analyzed in detail.

A series of measurements aimed at studying the optical-excitation functions of the calcium atomic states by means of electron impact was also performed at higher energies ( $E > 3$  eV). Ehlers and Gallagher [50] measured the absolute excitation cross-sections for  $4p$   ${}^1P^\circ$  emission at a wavelength of 422.7 nm with an energy resolution of about 0.3 eV. The structure observed by them in both the excitation cross-section and the linear polarization fraction adjacent to the threshold region for higher excited states was attributed to cascade transitions from some of those states. One cannot rule out that some part of this structure is induced by resonances. Garga *et al.* [51] measured the optical-excitation functions for more than 25 excited calcium states with an energy resolution of 1.0–1.2 eV. They observed a large number of structures and noted that some of them can be associated with the decay of ADSs of the negative  $\text{Ca}^-$  ion. Given the resolution of those experiments and the lack of detailed information concerning the observed structures, they are not worth commenting on here.

Figure 4 illustrates the energy dependence of the ICS of elastic electron scattering at the Ca atom in the metastable state  $4s4p$   ${}^3P^\circ$ . This figure also demonstrates the contributions to the ICS from the partial  ${}^4,2S^e$ ,  ${}^4,2P^e$ ,  ${}^4,2D^e$ ,  ${}^4,2F^e$ ,  ${}^4,2P^\circ$ ,  ${}^4,2D^\circ$ , and  ${}^4,2F^\circ$  waves. Above the excitation threshold of the  $4s4p$   ${}^3P^\circ$  level, the main contribution to this ICS is given by the partial  ${}^4,2P^e$  and  ${}^4D^e$  waves. As can be seen from Fig. 4, distinctly pronounced structures, which could be interpreted as resonances, are observed in the energy dependence of ICS. In particular, the sharp maximum in the  ${}^4F^\circ$  symmetry is associated with the  $4s4p[{}^3P]3d$   ${}^4F^\circ$  shape resonance (see Tables 3 and 5). This conclusion will be confirmed below while analyzing the energy dependence of the eigenphase sum.

The dominant process at  $E < 1.892$  eV is the elastic electron scattering by the Ca atom in the ground state. As one can see from Fig. 5, *a* (left panel), three resonance-like structures in the vicinity of energies of 1.15, 1.9, and 2.004 eV can be clearly distin-

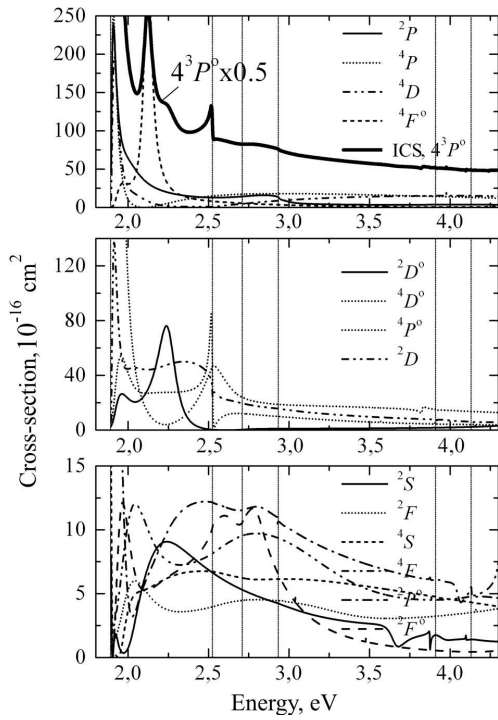


**Fig. 4.** The ICSs of elastic electron scattering by the calcium atom in the  $4s4p\ ^3P^o$  metastable state (bold solid curve). The contributions of various partial waves to the ICS of elastic  $e + Ca$  scattering are shown in the graphical panels. Vertical thin lines mark the excitation thresholds of Ca atom

guished in the energy dependences of the partial  $^2D^e$  cross-sections of elastic electron scattering at the Ca atom in the ground  $4s^2\ ^1S$  and metastable  $4s4p\ ^3P^o$  states and the  $4s^2\ ^1S - 4s4p\ ^3P^o$  transition excitation, respectively. The distances between the resonance peaks (with identical  $L = D$ ) in those energy dependences are quite small and approximately equal to 0.1 and 0.75 eV. The behavior of the energy dependences of the sum of partial  $^2D$  phases (Fig. 5, b) and its energy derivative (Fig. 5, c) also demonstrates that three resonance features ( $4s^2 3d\ ^2D$ ,  $4s4p[3P]4f\ ^2D$ , and  $4s4p^2\ ^2D$ ) overlap in a narrow energy interval of 1.1–2.0 eV, which stimulates a purely destructive picture of interference in the vicinity of those resonances.

Inelastic electron scattering by Ca atoms becomes appreciable at energies exceeding 1.892 eV. Figure 5, a (right panel) demonstrates the results of BSR39 calculations of the partial  $D^e$  excitation cross-sections for the  $4s^2\ ^1S - 4s4p\ ^3P^o$ ,  $4s^2\ ^1S - 3d4s\ ^1D^e$ ,  $4s^2\ ^1S - 4s4p\ ^1P^o$ ,  $4s^2\ ^1S - 4s5s\ ^3S^e$ ,  $4s4p\ ^3P^o - 3d4s\ ^3D^e$ , and  $4s4p\ ^3P^o - 3d4s\ ^1D^e$  transitions.

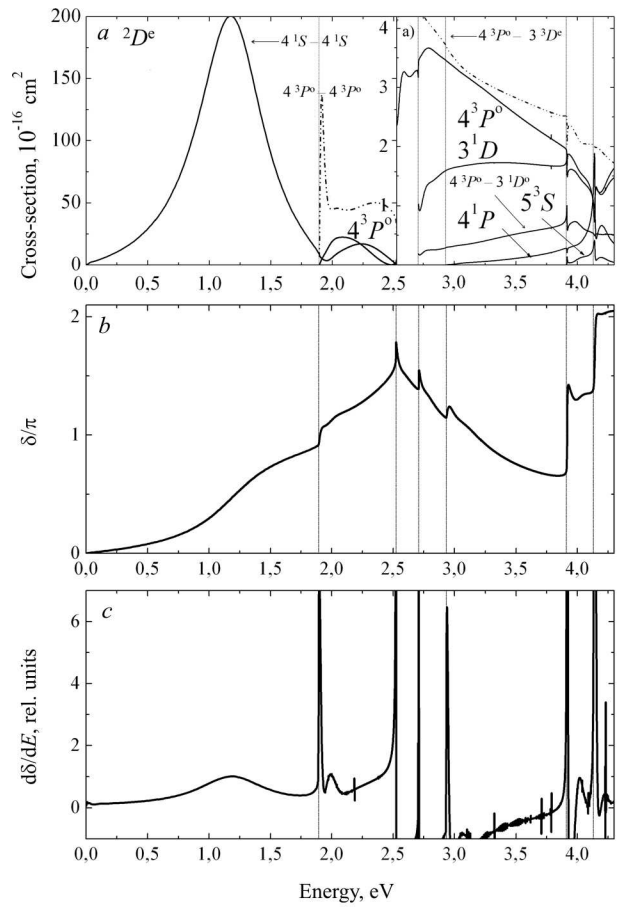


**Fig. 5.** Left panel: contributions of the partial  $^2D^e$  wave to the cross-sections of elastic electron scattering by the Ca atom in the ground  $4s^2\ ^1S$  and metastable  $4s4p\ ^3P^o$  states and excitation of various transitions (a):  $4s^2\ ^1S - 4s4p\ ^3P^o$  (left panel);  $4s^2\ ^1S - 4s4p\ ^3P^o$ ,  $4s^2\ ^1S - 3d4s\ ^1D^e$ ,  $4s^2\ ^1S - 4s4p\ ^1P^o$ ,  $4s^2\ ^1S - 4s5s\ ^3S^e$ ,  $4s4p\ ^3P^o - 3d4s\ ^3D^e$ , and  $4s4p\ ^3P^o - 3d4s\ ^1D^e$  (right panel). Energy dependence of the sum of partial  $^2D^e$  phases  $\delta$  (b). Energy dependence of the derivative  $d\delta/dE$  (c)

$3d4s\ ^3D^e$ , and  $4s4p\ ^3P^o - 3d4s\ ^1D^e$  transitions. As one can see from this figure, the inelastic contribution of the partial  $^2D$  wave to the excitation cross-sections of the energy levels of the Ca atom is essential only for the  $4s4p\ ^3P^o - 3d4s\ ^3D^e$ ,  $4s^2\ ^1S - 4s4p\ ^3P^o$ , and  $4s^2\ ^1S - 3d4s\ ^1D^e$  transitions, whereas this contribution is relatively small for other transitions (see Fig. 5, a).

At low collision energies, only a few partial phases are essentially different from zero. They can be calculated by numerically integrating the system of integro-differential equations (9) over  $r$  from the co-

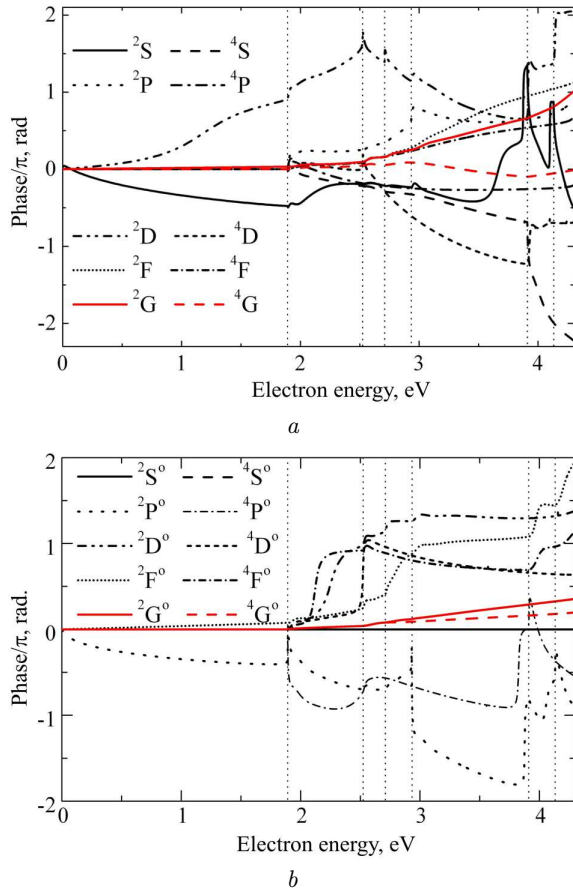


**Fig. 6.** Partial phases of electron scattering by the calcium atom for even (a) and odd (b) terms

ordinate origin to a distance  $r > a$  and equating the resulting solution to asymptotic expression (22). The partial phases of  $e + \text{Ca}$  scattering, which were determined in this way using the software package [32], are presented in Fig. 6 for both even (upper panel) and odd (lower panel) terms. The behavior of these partial phases in the vicinity of the corresponding resonance energies confirms the data quoted in Tables 3 to 5 for the resonance structure of the partial and integral cross-sections of  $e + \text{Ca}$  scattering.

The energy dependences of the total-cross-section derivative  $d\sigma(E)/dE$  measured experimentally [18, 19] and calculated by us in the BSR approximation are compared in Fig. 7. As can be seen from this figure, the structure of the resonance features in the  $d\sigma(E)/dE$  dependence can be traced more clearly than in the energy dependence of the cross-section itself,  $\sigma(E)$ . The irregularities observed in these en-

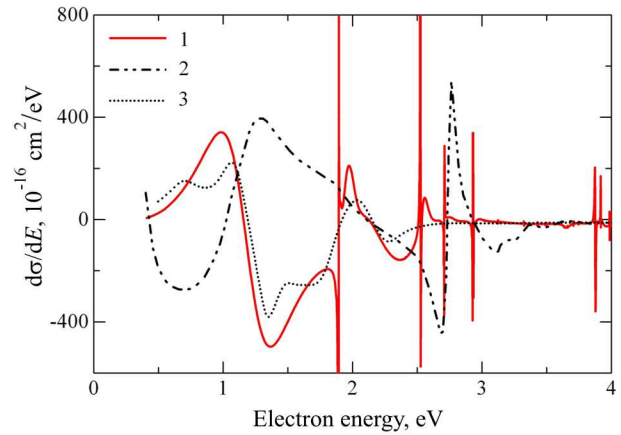


**Fig. 7.** Energy derivatives  $d\sigma/dE$  of the total cross-sections of electron scattering by the calcium atom: our BSR39 calculation (1), calculated according to experimental data by Johnson *et al.* [18] (2), calculated according to experimental data by Romaniuk *et al.* [19] (3)

ergy dependences (drastic jumps, as well as smooth maxima and minima) arise from the existence of resonances in some partial waves and from the threshold features in the cross-section itself. In particular, in the behavior of the energy dependences of the derivative  $d\sigma(E)/dE$ , three distinctly pronounced features are observed in the form of broad powerful structures in the vicinity of energies of 1.15, 1.9, and 2.004 eV, which could be interpreted as the above-threshold shape resonances, with characteristic narrow peaks of Feshbach resonances being superimposed on two gentle protrusions at 1.9 and 2.6 eV.

At even higher energies ( $E > 2.6$  eV), there arise a substantial number of narrow resonance peaks, which cannot yet be identified experimentally. Note also that the energy positions of the features in the energy dependences of the derivative  $d\sigma(E)/dE$  obtained experimentally [19] and calculated by us in the BSR39 approximation correlate well if the experimental curve is shifted to the right by 0.35 eV. At the same time, the experimental results of work [18] seem to be unreliable because the measured signal is proportional to the derivative of the transmission current only at low pressures, which was not maintained in the experiment [18]. Therefore, when elucidating the resonance structure of the ICS of  $e + \text{Ca}$  scattering, it is more acceptable to use the results obtained in work [19] and corrected in work [6] rather than the experimental data of work [18].

## 5. Conclusions

The performed research makes it possible to conclude that the BSR version of the  $R$ -matrix method, which was developed in our works [6–13, 21–26], is a universal and very efficient method to study elementary processes of interaction between slow electrons and complex multielectron atoms and ions. In comparison with the standard  $R$ -matrix method [16, 17], the proposed BSR version has three undeniable advantages:

1) the application of term-dependent nonorthogonal orbitals is the most advantageous way to take into account resonance effects without involving any correlation functions and without enlarging the system of integro-differential strong-coupling equations (9);

2) the relevant quantum-mechanical operators, after their discretization in the  $B$ -spline basis, are represented by sparse band finite-rank matrices, which significantly simplifies the solution of the corresponding systems of algebraic and integro-differential equations;

3) the local properties and the completeness of the finite system of basis splines guarantee the convergence of the  $R$ -matrix expansion, which allows us to exclude the necessity to introduce the Buttler corrections to the diagonal elements of the  $R$ -matrix [35].

A large body of detailed results of BSR calculations was obtained for the total and partial cross-sections (integrated over the scattering angle) of elastic electron scattering by the Ca atom in the ground  $4s^2\ ^1S$  and metastable  $4s4p\ ^3P^o$  states and the excitation of the transitions  $4s^2\ ^1S - 4s4p\ ^3P^o$ ,  $4s^2\ ^1S - 3d4s\ ^3D$ ,  $4s^2\ ^1S - 3d4s\ ^1D$ ,  $4s^2\ ^1S - 4s4p\ ^1P^o$  and  $4s^2\ ^1S - 4s5s\ ^3S$ . This enabled us to carefully analyze the influence of various physical factors – such as multi-electron correlations, resonance effects, interaction of discrete states with continuous spectrum, and the relaxation of the quantum orbit of excited electron – on the parameters of electron interaction with Ca atoms. The contributions of the partial  $^2S^e$ ,  $^2P^o$ ,  $^2D^e$ , and  $^2F^o$  waves to the angle-integrated total cross-sections of elastic scattering and excitation of most important electronic transitions in the Ca atom were calculated. This allowed us to unambiguously identify the origin of the characteristic structures in the energy dependences of the elastic scattering and excitation cross-sections for five lowest levels of the Ca atom.

To identify and classify resonances, the energy dependences of the  $e + \text{Ca}$  scattering cross-sections  $\sigma(E)$  and their energy derivatives  $d\sigma(E)/dE$  were analyzed in detail for every fixed  $L$  and parity. It was found that resonances are observed more pronounced in the derivatives than in the cross-section itself. It occurs because a large number of resonances with different symmetries overlap by energy and strongly interfere with one another in the total cross-section.

The role of autodetachment states of the negative  $\text{Ca}^-$  ion in the electron scattering by Ca atoms was studied and it was shown that the contribution of resonance processes to the cross-sections of elastic  $e + \text{Ca}$  scattering and Ca excitation is rather substantial at the quantitative level. In order to unambiguously identify the resonances at  $e + \text{Ca}$  scattering and obtain relevant information, we used the method of “complete separation of resonance and non-resonance channel spaces” [31]. The application of this method to  $e + \text{Ca}$  scattering made it possible to detect and identify 56 possible resonance states of the negative  $\text{Ca}^-$  ion and each of them was assigned a certain configuration (see Tables 3 to 5). The positions and widths of detected resonances were determined and their spectroscopic classification was performed. The existence of 11 resonances for which the phase jump in the vicinity of the resonance energy is close to  $\pi$  (see Table 5) was confirmed by other authors both experimentally [18–20] and theoretically [39–41].

The positions of reliably established resonances (see Table 5) are as follows:

- the resonance  $4s^23d\ ^2D$  is located below the excitation threshold of the level  $^3P^o$ ;
- the resonances  $4s4p[^3P]3d\ ^4F^o$ ,  $4s3d[^3D]4p\ ^2D^o$ , and  $4s4p[^3P]3d\ ^4D^o$  are located between the  $^3P^o$  and  $^3D$  thresholds;
- the resonances  $4s3d[^1D]4d\ ^2S$ ,  $4s5s[^3S]5p\ ^2P^o$ ,  $4s5s^2\ ^2S$ , and  $4s5s[^3S]5p\ ^2P^o$  are located between the  $^1P^o$  and  $^3S$  thresholds;
- the resonances  $4s5s[^3S]4d\ ^2D$  and  $4s5s[^1S]6s\ ^2S$  are located between the  $^3S$  and  $^1S$  thresholds;
- the resonance  $4s5s[^1S]4d\ ^2D$  is located above the  $^1S$  threshold.

As one can see from Tables 3 to 5, in the case of  $e + \text{Ca}$  scattering, the resonances are arranged very close to each other and most of them are rather narrow. Therefore, for their experimental confirmation, high-resolution equipment is required. Experimental results obtained for monoenergetic electron beams

and Ca atoms in the resonance energy interval will also be very valuable.

*The authors express their gratitude to Prof. O. Zatsarinny and Prof. K. Bartschat (Drake University, Des Moines, Iowa, USA) for their help in calculations and fruitful discussion.*

1. O. Zatsarinny, H. Parker, K. Bartschat. Electron-impact excitation and ionization of atomic calcium at intermediate energies. *Phys. Rev. A* **99**, 012706 (2019).
2. J.L. Hall. Nobel lecture: defining and measuring optical frequencies. *Rev. Mod. Phys.* **78**, 1279 (2006).
3. V.E. Fortov, B.Y. Sharkov, H. Stocker. European facility for antiproton and Ion research (FAIR): The new international center for fundamental physics and its research program. *Phys.-Usp.* **55**, 582 (2012).
4. *Applied Atomic Collision Physics. Vol. 2: Plasmas*. Edited by C.F. Barnett, M.F.A. Harrison (Academic Press, 1984).
5. E.Yu. Remeta, O.B. Shpenik, Yu.Yu. Bilak. Elastic scattering of slow electrons by calcium atoms into the angle interval depending on the collision energy. *Zh. Tekhn. Fiz.* **71** (4), 13 (2001) (in Russian).
6. O. Zatsarinny, K. Bartschat, S. Gedeon, V. Gedeon, V. Lazur. Low-energy electron scattering from Ca atoms and photodetachment of Ca. *Phys. Rev. A* **74**, 052708 (2006).
7. S. Gedeon, V. Gedeon, V. Lazur, L. Bandurina. Partially integrated differential cross-sections of e+Ca scattering. In *Abstracts of the 9th European Conference on Atomic and Molecular Physics (ECAMP), 6–11 May 2007* (Crete, Greece, 2007).
8. S. Gedeon, V. Lazur. Low-energy electron scattering from calcium. In *Abstracts of the 40th Annual Conference of the European Group for Atomic Systems (EGAS), 2–5 July 2008* (Graz, Austria, 2008).
9. O. Zatsarinny, K. Bartschat, S. Gedeon, V. Gedeon, V. Lazur, E. Nagy. Cross sections for electron scattering from magnesium. *Phys. Rev. A* **79**, 052709 (2009).
10. O. Zatsarinny, K. Bartschat, S. Gedeon, V. Gedeon, V. Lazur, E. Nagy. Cross sections for electron scattering from magnesium. *J. Phys.: Conf. Ser.* **194**, 042029 (2009).
11. V. Gedeon, S. Gedeon, V. Lazur, E. Nagy, O. Zatsarinny, K. Bartschat. Electron scattering from silicon. *Phys. Rev. A* **85**, 022711 (2012).
12. O. Zatsarinny, K. Bartschat, V. Gedeon, S. Gedeon, V. Lazur, E. Nagy. Electron scattering from silicon. In *Abstracts of the 43rd Annual Meeting of the APS Division of Atomic, Molecular and Optical Physics (DAMOP12), 4–8 June 2012* (Orange County, California, 2012).
13. V. Gedeon, S. Gedeon, V. Lazur, E. Nagy, O. Zatsarinny, K. Bartschat. *B*-spline *R*-matrix-with-pseudostates calculations for electron-impact excitation and ionization of fluorine. *Phys. Rev. A* **89**, 052713 (2014).
14. D.J. Pegg, J.S. Thompson, R.N. Compton, G.D. Alton. Evidence for a stable negative ion of calcium. *Phys. Rev. Lett.* **59**, 2267 (1987).
15. C.F. Fischer, J.B. Lagowski, S.H. Vosko. Ground states of Ca<sup>-</sup> and Sc<sup>-</sup> from two theoretical points of view. *Phys. Rev. Lett.* **59**, 2263 (1987).
16. P.G. Burke, W.D. Robb. The *R*-matrix theory of atomic processes. *Adv. At. Mol. Phys.* **11**, 143 (1976).
17. P.G. Burke. *R-matrix Theory of Atomic Collisions* (Springer, 2011).
18. A.R. Johnston, G.A. Gallup, P.D. Burrow. Low-lying negative-ion states of calcium. *Phys. Rev. A* **40**, 4770 (1989).
19. N.I. Romanyuk, O.B. Shpenik, I.P. Zapesochnyi. Cross sections and characteristics of electron scattering by calcium, strontium, and barium atoms. *JETP Lett.* **32**, 452 (1980).
20. N.I. Romanyuk, O.B. Shpenik, F.F. Papp, I.V. Chernysheva, I.A. Mandi, V.A. Kelemen, E.P. Sabad, E.Yu. Remeta. Study of low-energy scattering of electrons by Mg and Ca atoms using an optimized trochoidal spectrometer. *Ukr. Fiz. Zh.* **37**, 1639 (1992) (in Russian).
21. V. Gedeon, S. Gedeon, V. Lazur, E. Nagy, O. Zatsarinny, K. Bartschat. *B*-spline *R*-matrix-with-pseudostates calculations for electron collisions with aluminum. *Phys. Rev. A* **92**, 052701 (2015).
22. O. Zatsarinny, K. Bartschat, E. Nagy, S. Gedeon, V. Gedeon, V. Lazur. Electron scattering from aluminum: *B*-spline *R*-matrix calculations. *J. Phys.: Conf. Ser.* **635**, 052012 (2015).
23. O. Zatsarinny, K. Bartschat, E. Nagy, V. Gedeon, V. Lazur. Low-energy outer-shell photodetachment of the negative ion of aluminum. *J. Phys.: Conf. Ser.* **875**, 022003 (2017).
24. V. Gedeon, S. Gedeon, V. Lazur, O. Zatsarinny, K. Bartschat. Low-energy outer-shell photo-detachment of the negative ion of aluminum. *J. Phys. B* **51**, 035004 (2018).
25. E.A. Nagy, V.F. Gedeon, S.V. Gedeon, V.Yu. Lazur. Electron-impact excitation of 5<sup>1</sup>S – 5<sup>1</sup>P<sup>o</sup> resonance transition in Sr atom. *Ukr. J. Phys.* **63**, 11 (2018).
26. N.Yu. Kondor, O.V. Yegiazarian, V.Yu. Lazur. Calculations of the energy structure of P, S atoms by the *R*-matrix method with *B*-splines. *Nauk. Visn. Uzhgorod. Nats. Univ. Ser. Fiz.* **48**, 67 (2020) (in Ukrainian).
27. A. Igarashi, N. Toshima, T. Shirai. Muon transfer and elastic scattering in *t*+*dμ* collisions at low energies. *Phys. Rev. A* **50**, 4951 (1994).
28. A. Igarashi, I. Shimamura. Time-delay matrix analysis of resonances: application to the positronium negative ion. *J. Phys. B* **37**, 4221 (2004).
29. I. Shimamura, J.F. McCann, A. Igarashi. Eigenvalues of the time-delay matrix in overlapping resonances. *J. Phys. B* **39**, 1847 (2006).
30. K. Aiba, A. Igarashi, I. Shimamura. Time-delay matrix analysis of several overlapping resonances: applications to the helium atom and the positronium negative ion. *J. Phys. B* **40**, F9 (2007).

31. I. Shimamura. Complete separation of resonance and non-resonance channel spaces. *J. Phys. B* **44**, 201002 (2011).
32. O. Zatsarinny. BSR: *B*-spline atomic *R*-matrix codes. *Comput. Phys. Commun.* **174**, 273 (2006).
33. C. Bloch. Une formulation unifiée de la théorie des réactions nucléaires. *Nucl. Phys.* **4**, 503 (1957).
34. O. Zatsarinny, K. Bartschat. The *B*-spline *R*-matrix method for atomic processes: application to atomic structure, electron collisions and photoionization. *J. Phys. B* **46**, 112001 (2013).
35. P.J.A. Buttle. Solution of coupled equations by *R*-matrix techniques. *Phys. Rev.* **160**, 719 (1967).
36. S. Gedeon, V. Lazur. The calculations of cross sections of electron scattering on Calcium atom. *Nauk. Visn. Uzhgorod. Nats. Univ. Ser. Fiz.* **25**, 130 (2009).
37. O. Zatsarinny, C. Fischer. Atomic structure calculations using MCHF and BSR. *Comput. Phys. Commun.* **180**, 2041 (2009).
38. C. Froese Fischer, T. Tachiev. Allowed and spin-forbidden electric dipole transitions in Ca I. *Phys. Rev. A* **68**, 012507 (2003).
39. J. Yuan, L. Fritsche. Electron scattering by Ca atoms and photodetachment of Ca<sup>-</sup> ions: An *R*-matrix study. *Phys. Rev. A* **55**, 1020 (1997).
40. J. Yuan, C.D. Lin. Effect of core-valence electron correlation in low-energy electron scattering with Ca atoms. *Phys. Rev. A* **58**, 2824 (1998).
41. J. Yuan. Core-valence electron correlation effects in photodetachment of Ca<sup>-</sup> ions. *Phys. Rev. A* **61**, 012704 (1999).
42. *NIST Atomic Spectra Database*.
43. W.L. Wiese, J.R. Fuhr, T.M. Deters. Atomic transition probabilities of carbon, nitrogen, and oxygen: a critical data compilation. *J. Phys. Chem. Ref. Data Monogr.* **7**, 522 (1996).
44. J.R. Taylor. *Scattering Theory: The Quantum Theory on Nonrelativistic Collisions* (John Wiley and Sons, Inc., 1972).
45. F. Nitchitiu. *Phase Shift Analysis in Physics of Nuclear Interactions* (Mir, 1983) (in Russian).
46. F.T. Smith. Lifetime matrix in collision theory. *Phys. Rev.* **118**, 349 (1960).
47. K. Bartschat, P.G. Burke. Resfit-A multichannel resonance fitting program. *Comput. Phys. Commun.* **41**, 75 (1986).
48. K. Bartschat, M.J. Kushner. Electron collisions with atoms, ions, molecules, and surfaces: fundamental science empowering advances in technology. *Proc. Natl. Acad. Sci.* **113**, 7026 (2016).
49. S.M. Kazakov, O.V. Khristoforov. Resonance scattering of low-energy electrons by calcium atoms. *Zh. Tekhn. Fiz.* **55**, 795 (1985) (in Russian).
50. V.J. Ehlers, A. Gallagher. Electron excitation of the calcium 4227-Å resonance line. *Phys. Rev. A* **7**, 1573 (1973).
51. I.I. Garga, I.S. Aleksakhin, V.P. Starodub, I.P. Zape-sochnyi. Excitation of alkaline-earth atoms by the electron impact. *Opt. Spektrosk.* **37**, 843 (1974) (in Russian).

Received 25.02.22.

Translated from Ukrainian by O.I. Voitenko

В.Ф. Гедєон, В.Ю. Лазур,  
С.В. Гедєон, О.В. Єгізарян

РЕЗОНАНСНА СТРУКТУРА  
ПЕРЕРІЗІВ РОЗСІЯННЯ ПОВІЛЬНИХ  
ЕЛЕКТРОНІВ НА АТОМІ КАЛЬЦІЮ

З використанням розширеної БСР-версії *R*-матричного методу проведено систематичне дослідження розсіяння електронів на нейтральному атомі кальцію в діапазоні енергій зіткнення до 4,3 еВ. Для точного представлення хвильових функцій мішені використовується метод сильного зв'язку з наборами залежних від терму неортогональних орбіталей та сплайн-представленнями для базисних функцій. Розклад для сильного зв'язку включає 39 зв'язаних станів нейтрального кальцію, що охоплюють усі стани від основного до  $4s8s^1S$ . Детально досліджено складну резонансну структуру проінтегрованих за кутом повних перерізів пружного  $e + \text{Ca}$ -розсіяння та збудження станів  $4s4p^3P^o$ ,  $3d4s^3D^e$ ,  $3d4s^1D^e$ ,  $4s4p^1P^o$  і  $4s5s^3S^e$  атома Ca електронним ударом. Спостережувані структури пов'язано з конкретними автовідривними станами системи налітаючий електрон + атом Ca. Визначено положення і ширини виявлених резонансів та проведено їхню спектроскопічну класифікацію.

*Ключові слова:* електрон, атом кальцію, розсіяння, збудження, іонізація, метод *R*-матриці з *B*-сплайнами, неортогональні орбіталі, резонанси.